

Discovery of Cyclic Acylguanidines as Highly Potent and Selective β -Site Amyloid Cleaving Enzyme (BACE) Inhibitors: Part I—Inhibitor Design and Validation^{||,1}

Zhaoning Zhu,^{*,†} Zhong-Yue Sun,[†] Yuanzan Ye,[†] Johannes Voigt,[§] Corey Strickland,[§] Elizabeth M. Smith,[†] Jared Cumming,[†] Lingyan Wang,[†] Jesse Wong,[†] Yu-Sen Wang,[§] Daniel F. Wyss,[§] Xia Chen,[‡] Reshma Kuvelkar,[‡] Matthew E. Kennedy,[‡] Leonard Favreau,[†] Eric Parker,[‡] Brian A. McKittrick,[†] Andrew Stamford,[†] Michael Czarniecki,[†] William Greenlee,[†] and John C. Hunter[‡]

[†]Department of Medicinal Chemistry, [‡]Department of Neurobiology, and [§]Department of Structural Chemistry, Schering-Plough Research Institute, 2015 Galloping Hill Road, Kenilworth, New Jersey 07033

Received September 21, 2009

A number of novel amidine containing heterocycles were designed to reproduce the unique interaction pattern, revealed by X-ray crystallography, between the BACE-1 catalytic diad and a weak NMR screening hit (**3**), with special attention paid to maintaining the appropriate basicity and limiting the number of H-bonding donors of these scaffolds. The iminohydantoin cores (**10** and **23**) were examined first and found to interact with the catalytic diad in one of two binding modes (A and B), each with the iminohydantoin core flipped 180° in relation to the other. The amidine structural motif within each core forms a bidentate interaction with a different aspartic acid of the catalytic diad. Both modes reproduced a highly conserved interaction pattern between the inhibitors and the catalytic aspartates, as revealed by **3**. Potent iminohydantoin BACE-1 inhibitors have been obtained, validating the molecular design as aspartyl protease catalytic site inhibitors. Brain penetrant small molecule BACE inhibitors with high ligand efficiencies have been discovered, enabling multiple strategies for further development of these inhibitors into highly potent, selective and in vivo efficacious BACE inhibitors.

Introduction

Alzheimer's disease (AD^a) is a progressive, ultimately fatal neurodegenerative disease with an average life expectancy of 7–10 years after diagnosis.² It is the leading cause of dementia in the elderly population, causing gradual loss of mental and physical function. In addition to the devastating physical and emotional impact of AD on patients and their families, all patients at an advanced stage of the disease will inevitably need long-term care, which places a huge social and economic burden on their families and society.³ The combined Medicaid and Medicare cost of AD alone was projected to exceed 80 billion dollars in 2010.⁴ In the U.S. alone, there are currently 4 million AD patients with an additional 8 million subjects diagnosed with mild cognitive impairment (MCI), of whom many will progress to AD.⁵ This number is expected to quadruple in the next three decades unless therapies that impact the underlying pathophysiology of AD can be identified.

Current therapies for AD, comprising acetylcholine esterase inhibitors and an NMDA receptor antagonist, offer only symptomatic relief by compensating for the neuronal and synaptic losses in AD patients through prolonging activation

of the remaining neuronal network.⁶ These therapies offer patients transient improvements in cognition and daily living functions, but do not halt disease progression. Thus, there are enormous unmet medical needs for the AD population.

The pathological hallmarks observed in the brains of AD patients are the extracellular amyloid plaques, mainly composed of an amyloid β peptide with 42 amino acids in length (A β 42), and the intracellular neurofibrillary tangles of hyperphosphorylated τ protein. According to the amyloid hypothesis,⁷ the prevailing theory in the field, the underlying cause of AD is the aggregation and deposition of A β 42 in the brain due to its overproduction and/or diminished clearance. This hypothesis is supported by strong genetic, histopathological, and clinical evidence. All early onset familial AD is identified by genetic mutations in amyloid precursor protein (APP) or presenilins (PS1/PS2) that result in increased A β peptide production. Down's syndrome patients, who have an extra copy of chromosome 21 containing the APP gene, or individuals who have a duplication of only a portion of chromosome 21 that contains the APP gene, produce more A β peptides and develop early onset AD.⁸ One Down's individual,⁹ whose extra copy of the portion of chromosome 21 lacked the APP gene, did not develop AD. Among all β -amyloid species, A β 42 is most prone to aggregation and most cytotoxic in vitro.¹⁰ Lastly, active immunization against A β peptides reduced amyloid load in animal models¹¹ and was associated with cognitive improvement for AD patients who developed robust anti-A β titers in human clinical trials.¹²

A β peptides, ranging from 37 to 42 amino acids in length, differ from each other at the C-terminus. They are produced

^{||} New protein/ligand coordinates have been deposited in the PDB with ids of 3L58, 3L59, 3L5B, 3L5C, 3L5D, 3L5E, 3L5F.

^{*}To whom correspondence should be addressed. Phone: 908-740-5651. Fax: 908-740-7152. E-mail: Zhaoning.Zhu@spcorp.com.

^aAbbreviations: AD, Alzheimer's disease; APP, amyloid precursor protein; BACE, β -site amyloid precursor protein cleaving enzyme; CSP, chemical shift perturbation; HEA, hydroxyethylamine; SAR, structure–activity relationship; TEA, triethyl amine; TS, transition state; RFU, relative fluorescence units; ECL, electrochemiluminescence.

as minor products (5–10%) of the metabolism of the membrane bound APP via two consecutive cleavages, first by β -site APP cleaving enzyme (BACE-1, also known as β -secretase or memapsin-2),¹³ followed by γ -secretase. BACE-1 KO mice are normal, do not produce $A\beta$ peptides, and have few overt phenotypes.^{14,15} Crossing BACE-1 KO mice with transgenic mice that overproduce human APP eliminates $A\beta$ production and amyloid plaque formation and rescues memory dysfunction.¹⁶ These data suggest that $A\beta$ peptide inhibition through small molecule BACE-1 inhibitors is highly promising as a disease modifying therapy that may halt or even reverse the progression of AD.

BACE belongs to the aspartyl protease family with two aspartic acids constituting the catalytic diad. As the first identified BACE homologue, BACE-1 is mainly expressed in the central nervous system and is responsible for $A\beta$ peptide production. The other homologue, BACE-2, cleaves APP at a different site to the BACE-1 cleavage and is mainly expressed in the periphery.¹⁷ BACE-1 is an integral membrane protein localized within acidic (pH \sim 5) intracellular compartments with its active site intralumenally juxtaposed to its cleavage recognition site of APP.¹⁸ This acidic intralumenal space is an aqueous environment, thus an effective BACE-1 inhibitor must have sufficient hydrophobicity to pass through the blood–brain barrier and yet be sufficiently water-soluble to reach the aqueous acidic compartment where BACE-1 is active. Historically, brain penetrating and CNS active aspartyl protease inhibitors have been difficult to obtain.¹⁹

Early potent BACE-1 inhibitors represented by OM99–2 are substrate-based statine and homostatine peptide transition state (TS) mimetics with high molecular weights and unattractive overall molecular profiles.²⁰ Another known class of BACE-1 inhibitors is the hydroxyethyl amine (HEA) related TS mimetics represented by **1** and **2**, which

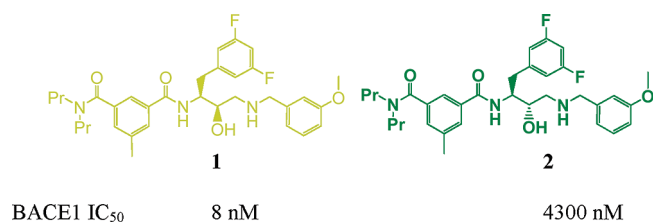


Figure 1. Representative HEA peptidic TS mimetic BACE-1 inhibitors. Both compounds are PGP substrates based on a CACO2 permeability ratio assay.

dominated the early BACE-1 inhibitor research literature (Figure 1).²¹ Inhibitors **1** and **2** have opposite stereochemistry of the hydroxyl group. [The –OH position in **2** is close to that in OM99–2 (BACE-1 IC₅₀ 2 nM; pdb code: 1fkf).] Superimposed X-ray coordinates, obtained at Schering-Plough, of **1** and **2** in BACE-1 (Figure 2) illustrate the nature of the tetrahedral intermediate mimicking the preceding TS of a water molecule adding to the amide carbonyl group through a general acid and general base mechanism.²² In addition, published and in-house research involving these highly potent peptidomimetic BACE-1 inhibitors has generated a detailed understanding of the BACE-1 enzyme and its important interactions and binding pockets available for inhibitor development. Among the major interactions, the 3,5-difluorobenzyl group in **1** resides in the S1 pocket and the *m*-methoxybenzyl stretches from the S1' toward S2' pocket. The basic secondary amine should be protonated, with one of its protons within hydrogen bonding distance of the top oxygen of the carboxylic acid of Asp²²⁸. One *n*-propyl group on the distal amide nitrogen of the isophthalamide group extends into the S3 subpocket (S3_{sp}). The distal amide carbonyl group of the isophthalamide forms a hydrogen bond with the amide proton of Thr²³². The front hairpin domain (flap) of BACE-1 is in a closed position with the phenol of Tyr⁷¹ forming an edge-to-face π – π stacking with the 3,5-difluorobenzyl group of **1**. It is in a well-ordered conformation with the electron density of its backbone and side chains clearly observed.

Many versions of the HEA design have been featured in work from multiple research groups across academia and industrial research laboratories. Unfortunately, most inhibitors from this class were found to lack oral bioavailability and brain penetration and many are substrates of P-glycoprotein (Pgp).²³ At the outset of our efforts, there were no known orally active BACE-1 inhibitors reported to reduce CNS $A\beta$ peptide production, and no small molecule nonpeptidomimetic BACE-1 inhibitors had been reported. Here we report an effort that led to a class of novel brain penetrating nonpeptidomimetic small molecule BACE-1 inhibitors.

Identification of 3 as a Novel BACE-1 Inhibitor through NMR Fragment Screening and Subsequent X-ray Crystallography Confirmation. Thioisourea **3** was identified as a novel BACE-1 active site inhibitor (Figure 3a) through a fragment-based NMR screening approach followed by confirmation with X-ray crystallography (Figure 3b).²⁴ This compound has a K_d of 15 μ M as determined by titration using ¹⁵N–H NMR chemical shift perturbation (CSP) and

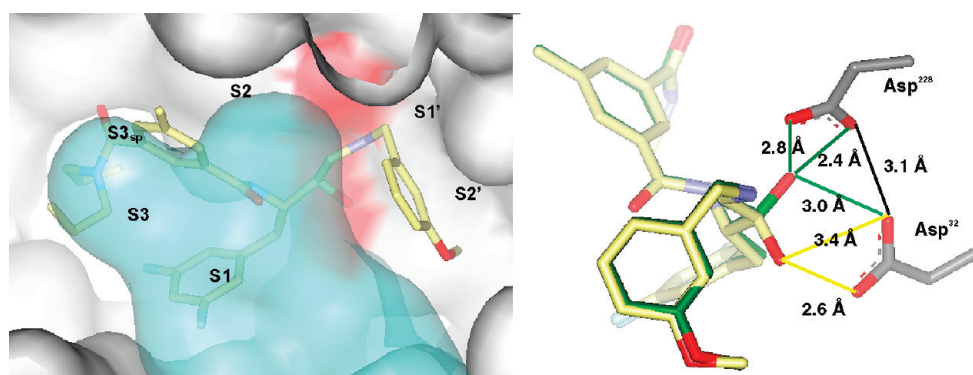


Figure 2. (left) X-ray structure of **1** (yellow) binding in the catalytic site of BACE-1 enzyme: red surface is the two catalytic aspartic acids (Asp³² and Asp²²⁸) and the blue surface is the flap, which is in the “closed” conformation. (right) Superimposed X-ray conformations of **1** (yellow) and **2** (green) with the key interactions with the catalytic diad of the BACE-1 enzyme: the two hydroxyl groups mimicking the tetrahedral intermediate.

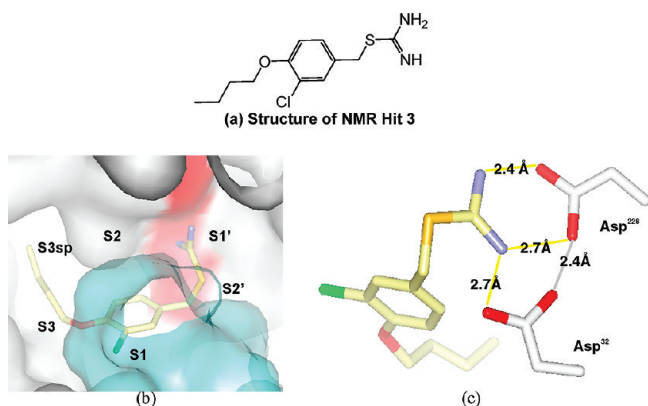


Figure 3. (a) Structure of **3**. (b) Compound **3** binding to the BACE-1 enzyme with the chlorophenyl in S1, butoxy group reaching in the S3 subpocket. (c) Detailed interaction of the amidine functionality with the catalytic diad of the BACE-1 enzyme.

an IC_{50} of 200 μM in an in vitro APP-peptide proteolysis assay with human soluble BACE-1.

The H-bonding interaction network between the amidine moiety and the aspartyl protease catalytic diad is highly unique as shown in Figure 3. Thioisourea **3** is basic, as *S*-methyl thioisourea, a close analog, was reported to have a pK_a value of 9.8.²⁵ At the optimum pH of BACE-1 (pH \sim 5), the ligand should be protonated at the binding site with two protons attached to each nitrogen atom. Each of the two nitrogen atoms of the amidine group is within hydrogen bonding distance with corresponding oxygen atom of the carboxylic acid of Asp²²⁸ (2.4 and 2.7 Å, respectively), forming a bidentate H-bonding interaction. The second proton from the lower nitrogen of **3** in Figure 3c is also hydrogen bonded to an oxygen of the carboxylic acid of Asp³² (2.7 Å). Only one of four protons of the protonated thioisourea is not directly interacting with the catalytic aspartic acids. The flap of BACE-1 is in a closed position with the phenol of Tyr⁷¹, forming an edge-to-face π - π stacking with the chlorophenyl group of **3**.²⁶

Structural chemical establishment of the novel BACE-1 inhibitors such as **3** and its hydrogen bond network with the catalytic diad of BACE-1 offered opportunities for an alternative inhibitor design to the TS mimetics represented by **1**. However, it presented a huge challenge to further develop these weak inhibitors. Foremost was whether any new BACE-1 inhibitor design based on the interaction pattern between thioisourea motif **3** and the catalytic aspartates would possess high enough intrinsic binding affinity to match the highly potent HEA class inhibitors. In addition, whether it would be possible to identify a drug candidate possessing such a structural motif as in **3** (Figure 2) that would achieve appropriate orally bioavailability and CNS penetration, a feature that is required for a BACE inhibitor, was uncertain.

Inhibitor Design. We assumed the basicity of **3** to be important and that it would be necessary to preserve the basic amidine functionality in the new BACE inhibitor design in order to reproduce its unique interactions with the catalytic aspartic acids. Mixed quantum and molecular mechanics (QM/MM) calculations suggested that both catalytic aspartic acids are deprotonated when bound to the protonated basic amidine motif of **3**.²⁷ We speculated that the pK_a of the desired inhibitor should be above the operating pH of BACE-1 for efficient protonation (i.e., with

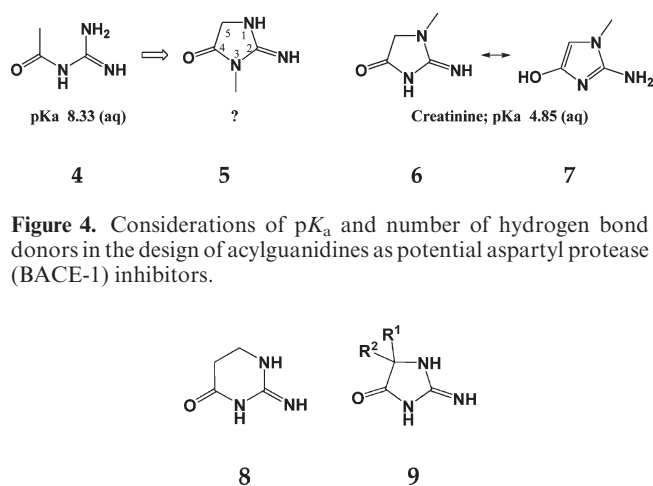


Figure 4. Considerations of pK_a and number of hydrogen bond donors in the design of acylguanidines as potential aspartyl protease (BACE-1) inhibitors.

With appropriate substitutions, cyclic acylguanidines such as iminopyrimidinone **8** and iminohydantoin **9** may be suitable pharmacophores for aspartyl protease inhibitors because of their basicity range and limited number of HB donors.

$pK_a > 5.0$). The thioisourea is an unattractive pharmacophore due to its susceptibility to oxidative degradation, chemical reactivity and toxicity.²⁸ On the other hand, simple amidines, especially these with unsubstituted nitrogens, are highly basic ($pK_a \sim 12$), a known factor that contributes to their low bioavailability.²⁹ According to an analysis by Lipinski et al., most CNS drugs are weakly basic and have two or fewer hydrogen bond donors.³⁰ We therefore wanted to identify an amidine bearing group with a pK_a ranging from 6 to 10. One of a few such groups is acylguanidine with a reported pK_a of 8.9,³¹ within the ideal range. However, the acylguanidine **4** is an equally unattractive pharmacophore with five hydrogen bond donors present at the protonated state. As illustrated in Figure 3c, three H-bond donors are crucial in order to maintain the interactions of the protonated ligand with the two aspartic acids of BACE-1, of which a minimum of two are present in the unprotonated free base form. Therefore, multiply substituted acylguanidines, and the cyclized versions in particular (e.g., **5** in Figure 4), should be a superior choice for optimization to a drug candidate.

However, a structurally related cyclic acylguanidine, creatinine (**6**), was found to have a pK_a of 4.85,³² a value that might be too low for **6** to be effectively protonated at the operating pH of BACE-1. While the dramatic differences in pK_a 's between acyclic (**4**) and cyclic acylguanidines (**6**) were at first surprising, we speculated that this may be a result of the increased acidity of the methylene group present in cyclic acylguanidines **5** and **6** due to its connectivity to the electronegative nitrogen and potential aromatic stabilization of tautomer **7**, a major structural difference from the basic acyclic acylguanidine **4**. On the other hand, we reasoned that cyclic acylguanidines, such as a six-membered dihydroiminopyrimidinone (**8**) or a 5,5-disubstituted five-membered iminohydantoin (**9**), would maintain the desired basicity (Figure 5).

We first focused on the iminohydantoin core in the design of BACE-1 inhibitors due to its ready accessibility from α,α -disubstituted aminoesters. In contrast to thioisourea **3**, iminohydantoin **9** has two positions for attachment of the benzyl group, i.e., from N3 or N1 to form two isomeric amidine structures (type I and type II, represented by **10** and **11**, respectively) (Figure 6). The *m*-chlorobenzyl group in **10** and **11** was adapted from compound **3** with truncation of the

n-butoxyl group. Both structure types were evaluated in ligand docking studies using the X-ray conformation of BACE-1 obtained from the crystal structure of thioisourea **3** in complex with the enzyme. Because it was not obvious that one of the designs would be superior to the other due to steric or electronic factors, we therefore decided to investigate both types of inhibitor designs.

Computational Evaluation of Type I and Type II BACE Inhibitors. After computational establishment that the protonated amidine motif binds to the doubly deprotonated aspartic acid catalytic diad, molecular docking studies of **10** and **11** with the coordinates of the crystal structure of **3** in complex with BACE were performed. The top ranking pose generated with Glide displayed the same amidine–aspartate

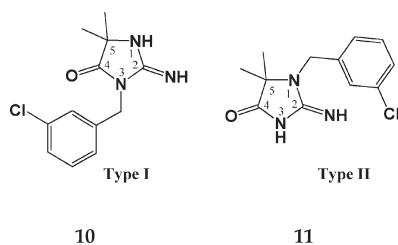
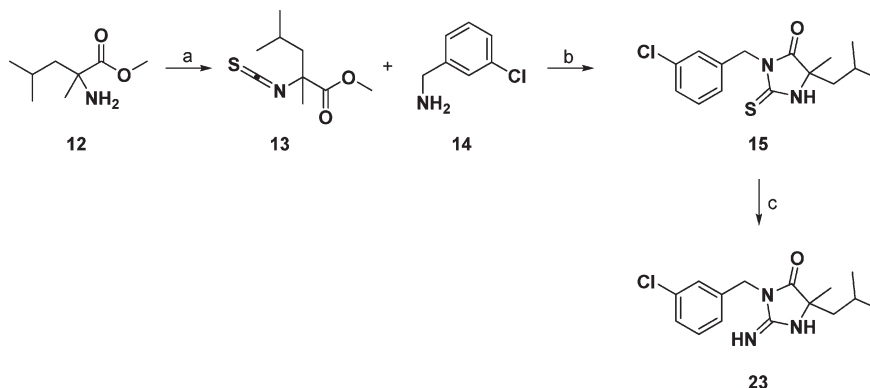


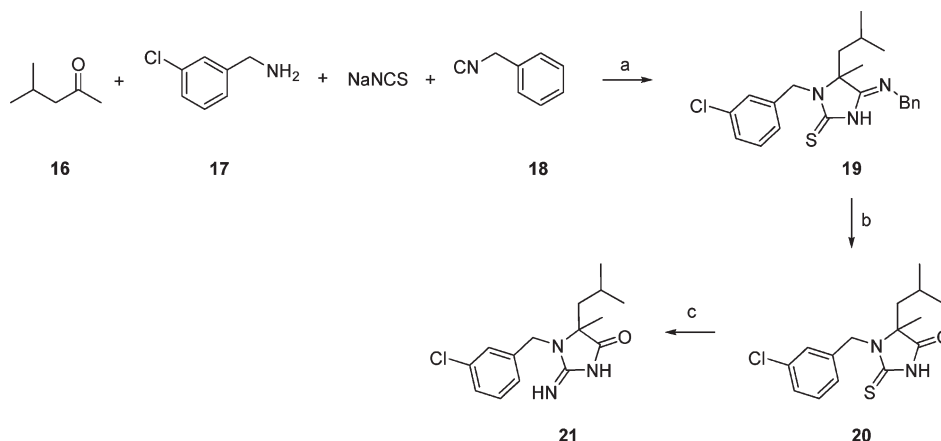
Figure 6. Two types of iminohydantoin (type I and type II) designs that preserve the crucial amidine functionality.

Scheme 1^a



^a(a) 1.2 Equiv thiocarbonyldipyridone, DCM; (b) DCM; (c) saturated aqueous ammonia, MeOH, *tert*-butylhydroperoxide.

Scheme 2^a



^a(a) methanol reflux; (b) 1:1 ethanol and conc HCl, μ W, 150°C; (c) ammonia in methanol and *tert*-butylhydroperoxide.

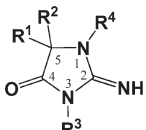
interactions as observed for **3** with the chlorophenyl group occupying S1 in both cases.

Synthesis of Type I and Type II Iminohydantoin. The synthesis of type I iminohydantoin is shown in Scheme 1. Aminoester **12** was treated with thiocarbonyldipyridone in DCM to give crude isothiocyanate **13**, which was reacted with *m*-chlorobenzylamine to give thiohydantoin **15**. Oxidative amination of **15** in aqueous methanolic ammonia and 5–10 equiv of aqueous *tert*-butylhydroperoxide overnight gave type I iminohydantoin **23** after workup and purification.³³

A parallel synthesis version of this procedure was developed to expedite the early phase of structure activity relationship (SAR) interrogation. Achiral α,α -disubstituted amino acid esters were synthesized using Bucherer–Bergs hydantoin synthesis starting from ketones followed by hydrolysis and esterification.³⁴ Chiral α,α -disubstituted amino acid esters were synthesized following known oxazolidinone chemistry described in the literature.³⁵

Type II iminohydantoin were synthesized from corresponding thiohydantoin (e.g., **21**), which were obtained from corresponding iminothiohydantoin (e.g., **20**) through multi-component coupling chemistry (Scheme 2).³⁶

NMR Chemical Shift Perturbation. 2D ¹⁵N-HSQC NMR was used to screen program compounds as mixtures of 10 at a concentration of 500 μ M in H₂O against ¹⁵N-labeled BACE-1 catalytic domain. Hits were identified by comparing two sets of ¹⁵N–H NMR spectra obtained with and

Table 1. Chemical Shift Perturbations of Iminoheterocycles and Percentage Inhibition of BACE-1 Enzyme in HTRF Assay^a


no.	R1	R2	R3	R4	class	protein CSP	BACE-1% inh @ 500 μ M
10	Me	Me	<i>m</i> -Cl-Bn	H	type I	very large	19
21	Me	isobutyl	H	<i>m</i> -Cl-Bn	type II	not observable	6
23	Me	isobutyl	<i>m</i> -Cl-Bn	H	type I	very large	55
24	Me	Me	H	<i>m</i> -Cl-phenethyl	type II	not observable	-20

^aCompounds **21** and **23** are racemic.

without cocktails of small molecule compounds. Clusters which caused chemical shift changes of active site residues of BACE-1 were deconvoluted to identify the hits.

In Vitro Biology. Inhibitor IC₅₀s were determined using time-resolved fluorescence end-point proteolysis assays with a human Swedish amyloid precursor protein peptide substrate (BACE-HTRF assay). BACE-mediated hydrolysis of this peptide results in an increase in relative fluorescence (RFU) at 620 nm after excitation with 320 nm light.

X-ray Crystallography. X-ray crystal structure of the complex of BACE-1 and compound **3** was obtained by co-crystallization. Crystal structures of further complexes were obtained by soaking the cocrystals of compound **2** in a solution containing the new compound for approximately 24 h.

Results and Discussions

A. SAR Development Using Chemical Shift Perturbation and Discovery of Two Binding Modes Using Protein X-ray Crystallography. The BACE-1 inhibition data for the first few iminohydantoin are listed in Table 1. These compounds were either inactive at the concentration tested or weakly active in the BACE-1 biochemical assay, with the best displaying modest percent BACE-1 inhibition at 500 μ M. However, protein NMR consistently indicated that the type I iminohydantoin, e.g., **10** and **23**, bound to the active site of BACE-1 and induced large chemical shift perturbations of the catalytic diad (Asp³²/Asp²²⁸) and other BACE-1 residues corresponding to different binding sites (Table 1). The NMR *K_d* values were determined to be 200 μ M for **10** and 123 μ M for **23**, averaged respectively over three values, each obtained from a different cross peak in the ¹⁵N-HSQC signal. These NMR data strongly suggested that iminohydantoin **10** and **23**, similar to thioisourea **3**, bind to the active site of BACE-1. On the other hand, none of type II inhibitors showed any chemical shift perturbation at the screening concentration (**21** and **24**, Table 1). This clear SAR, while not predicted, did provide some confidence in the reliability of the ¹⁵N-HSQC NMR data to guide the initial phase of SAR development.

More importantly, X-ray crystallography also corroborated the observations on the NMR chemical shift perturbations. The electron densities of compounds **10** and **23**, the first two type I iminohydantoin generated in this program, were clearly observed by X-ray crystallography with resolutions of 2.0 and 1.8 Å, respectively. On the other hand, a number of soaking experiments with type II iminohydantoin, e.g., compound **21** and **24**, were unsuccessful in generating observable inhibitor electron density within the

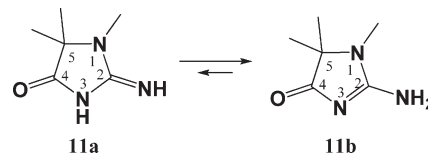


Figure 7. Type II iminohydantoin tautomer stabilities indicated that the N3 site needed to be blocked to maintain the basicity of these scaffolds.

BACE-1 substrate binding pocket. It was subsequently determined that type I iminohydantoin **23** has a *pK_a* value of 7.2, while type II iminohydantoin **24** has a *pK_a* value of 4.4,³⁷ suggesting that type II iminohydantoin would be predominately unprotonated under BACE-1 cocrystallization conditions and at the pH optimum of the enzyme. This supported the notion that the protonation state of the ligand is important, especially to these low molecular weight weak inhibitors that derive significant contribution of their affinity to BACE-1 from their interactions with the catalytic diad. Quantum mechanical calculations suggest that tautomer **11b** is likely to be preferred in aqueous solution over **11a** based on a 3 kcal/mol relative energy difference. Thus the imide N-H of protonated type II iminohydantoin **11** would be most acidic, which would explain the lower *pK_a* of **24** than that observed in **23** (Figure 7). Therefore, in order to maintain proper basicity, one would need to block the imide N-H.

The X-ray conformation of type I iminohydantoin **10** bound to BACE-1 reproduced the interaction pattern with the enzyme almost exactly as predicted by the docking model (Figure 8a). The amidine group forms the H-bond pattern with Asp³² and Asp²²⁸ as observed with thioisourea **3**. The chlorophenyl group resides in S1 forming hydrophobic interactions with side chains of Leu⁹¹, Ile¹⁸⁹, Trp¹⁷⁶, Ile¹⁷¹, and Phe¹⁶⁹. The flap is in a closed position with the phenol side chain of Tyr⁷¹, forming a face-to-edge interaction with the chlorophenyl of **10** (Figure 8c).

Although the structural difference between iminohydantoin **23** and **10**, in which one of the C-5 methyls in **10** is replaced with an isobutyl, may be considered minor, the X-ray structure of **23** bound to BACE-1 showed a binding mode completely different to that of **10**. The iminohydantoin core of **23** is flipped 180°, placing the isobutyl group in S1 and the chlorobenzyl group in S1' (Figure 8). Any concern about the seeming randomness of their X-ray conformations is quickly dispelled with a superimposition of the coordinates of both iminoheterocycle cores and the corresponding catalytic aspartic acids (Figure 8). The catalytic diad from X-ray structures of **10** and **23** are almost superimposable, and both iminohydantoin cores maintain the same hydrogen bonding

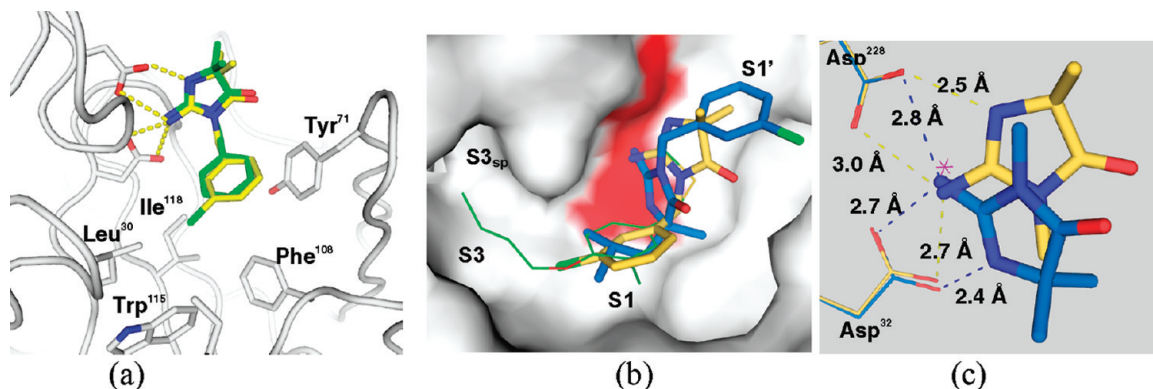


Figure 8. (a) X-ray conformation (yellow) of iminohydantoin **10** bound to the catalytic site of BACE-1 is almost identical with the computational docking prediction (green). The flap is in the closed position with Tyr⁷¹ side chain (dark gray) forming edge-to-face interaction with the chlorophenyl group of **10**. (b) Superimposed X-ray conformations of thioisourea **3** (green line), iminohydantoin **10** (yellow), and **23** (blue) with flap deleted for clarity. The red surface is the location of the aspartates. (c) Superimposed conformations of iminohydantoin cores of **10** (mode A) and **23** (mode B) and their detailed H-bonding patterns with Asp³² and Asp²²⁸. Notice the position of a highly conserved water molecule in the Apo protein (magenta, pdb code: 1w50).

network revealed by thioisourea **3**, with **10** (yellow) forming the bidentate interaction with Asp²²⁸, which is termed mode A, and **23** with Asp³², which is termed mode B. There is a near C₂ symmetry in the superimposed assemblies of ligand–diad conformations for **10** and **23** (Figure 8c). The exocyclic imino group of each ligand occupies an almost identical location to that of a highly conserved water molecule in the apo protein. This is a highly conserved feature observed within the X-ray structures of a variety of amidine containing BACE-1 inhibitors, indicating the imino moiety of the cyclic acylguanidine core, with its two H-bond donors, serves as the apo water replacement in addition to making other interactions within the catalytic site. Another significant difference between cocrystal X-ray structures of **10** and **23** is their respective flap conformation (not shown). The BACE-1 flap electron density was too weak to be observed in the enzyme complex with **23**, indicating an open and highly disordered position. Therefore, mode A inhibitors, with the well-ordered flap conformation observed with **10**, may be able to gain additional interactions through the closed flap position that are not available to Mode B iminohydantoin.

Binding modes A and B of type I iminohydantoin offered complementary opportunities to further improve the binding affinity of these weak ligands. Mode A inhibitors such as **10** (yellow in Figure 8b) may extend to the S1' and S2 pockets via *gem*-5,5-disubstitution. The chlorophenyl residing in S1 also afforded the opportunity to be extended into S3 and the S3 subpocket to optimize binding affinity. Mode B inhibitor **23**, with a preference for the isobutyl group in S1, occupied two conventional binding sites in BACE-1 (S1 and S1'). The isobutyl group residing in S1 should be amenable to further optimization and the C-5 methyl of **23** is well positioned for a larger group to extend to the S2' binding pocket.

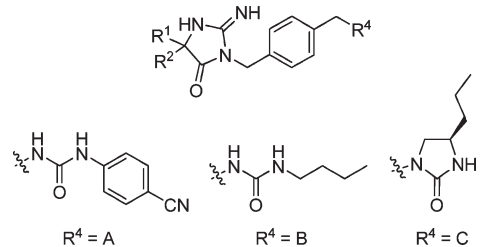
The reliance on the ¹⁵N–H NMR chemical shift perturbation data for SAR information due to the weak inhibitory activities of these early leads, and the unpredictable binding modes revealed by X-ray crystallography were some of the unique challenges to the early phase of SAR development of the iminohydantoin BACE-1 inhibitors. This clearly was not a conventional lead optimization effort where one would probe SAR with one well-designed structure at a time. We therefore adapted a high throughput synthesis strategy coupled with the medium throughput ligand–BACE-1

NMR chemical shift perturbation analysis that could explore one general SAR direction with a relatively large number of analogues at a time without the need to discern with high precision the assay outcome for any one specific compound.

The parallel synthesis chemistry enabled expeditious SAR development of type I iminohydantoin (scaffold **22**, R⁴ = H), varying both R¹ and R² groups, derived from the *gem*-disubstituted aminoacids and R³ that came from the amine component (see Scheme 1). Given our initial lack of understanding of the factors, such as structural variations of R¹/R² or R³, that might influence the preference for different binding modes, we decided to use racemic α,α -disubstituted aminoacids for SAR development and rely on X-ray crystallography for identification of the preferred stereochemistry and mode of binding once an inhibitor with improved affinity was found.

We first fixed R¹ and R² as methyl and isobutyl to scan the R³ SAR based on the observation that the isobutyl group of **23** in S1 is close to the position of the P1 isobutyl side chain of **OM99–2**. Over 500 different R³ groups were examined for their ability to cause the BACE-1 active site chemical shift perturbations. Type I iminohydantoin with a primary benzyl group at N3 (**10** in Figure 6) consistently demonstrated “very large” protein NMR ¹⁵N–H chemical shift perturbations of BACE-1 active site residues. Further exploration of substitutions on the benzyl group led to rapid improvement of potency for inhibition of BACE-1 protease activity in a short period of time (Table 2).

Compound **31** was the first compound to achieve μ M BACE-1 IC₅₀ (7 μ M) and was identified as a mode A inhibitor using X-ray crystallography (Figure 9). The iminohydantoin core is in a position similar to the amidine moiety of thioisourea **3** and iminohydantoin **10**. The 5-isobutyl group is projected toward the S1' pocket, and its electron density was too weak to be observed. The N3-benzyl group resides in S1 with the extended *p*-cyanophenyl urea from the para position of the benzyl, forming two H-bonding interactions with the carbonyl groups of Lys¹⁰⁷ and Phe¹⁰⁸ (Figure 9b). The *p*-cyanophenyl clearly improved binding affinity in comparison with the *N*-butyl urea **32** (Table 2) despite the fact that its electron density (and that of the Lys¹⁰⁷ side chain) was not observed. A number of *N*-aryl ureas related to **31** consistently demonstrated the importance of the aryls (but not related

Table 2. SAR Developments


no.	R ¹	R ²	R ⁴	BACE-1 IC ₅₀ (nM)	C5 center
31	<i>i</i> -Bu	Me	A	7000 ^a	racemic
32	<i>i</i> -Bu	Me	B	~78000	racemic
33	cyclohexylmethyl	Me	B	5000 ^a	racemic
34	Bn	Me	B	64% Inh. at 500 μM	racemic
35	cyclohexylmethyl	cyclohexylmethyl	B	2100 ^a	racemic
36	<i>i</i> -Bu	phenethyl	B	50000	racemic
37	<i>i</i> -Bu	cyclohexylethyl	B	3000 ^a	racemic
38	cyclohexylmethyl	cyclohexylethyl	B	350 ^a	racemic
39	cyclohexylmethyl	cyclohexylethyl	C	27 ^a	(R)

^a Each IC₅₀ value is an average of three determinations and the standard errors for all IC₅₀ determinations are less than 10%.

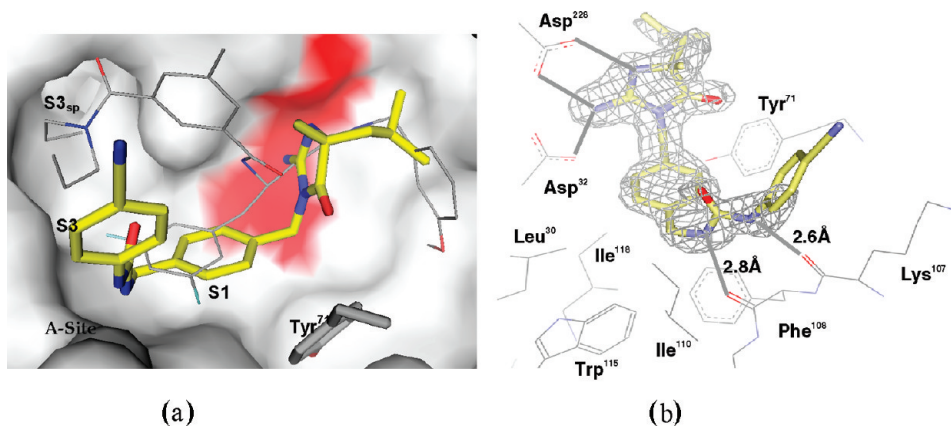


Figure 9. (a) Superimposed X-ray structures of HEA inhibitor **1** (gray line) and mode A inhibitor **31** (yellow); the flap is in a closed position. (b) Detailed H-bonding interactions of iminoheterocycle of **31** with the catalytic diad and additional H-bonding interactions picked up by the urea group with Lys¹⁰⁷ and Phe¹⁰⁶. Note that the density of the isobutyl and the *p*-cyanophenyl (light blue wire mesh) is too weak to be observed.

alkyls) to the BACE-1 inhibitory activity despite the fact that they all reside in this highly solvent exposed area. The *N*-aryl aromatic group and the alkyl side chain of the Lys¹⁰⁷ are in close proximity, suggesting hydrophobic packing of the aryl group against methylenes of the charged lysine side chain. This site to which the phenyl urea moiety binds is unique and was found to be repeatedly occupied during subsequent inhibitor SAR development. We have therefore named it “the A-site” after the fact that it was first discovered with a mode A inhibitor (**10**).³⁸ The flap is in the closed position with the phenol side chain of Tyr⁷¹ electron density, but not the remainder of the flap that is observable, indicating a large degree of flap motion.

Compound **32**, on the other hand, was found to be a mode B inhibitor (Figure 10) that occupies two binding pockets of the BACE-1 enzyme (S1 and S3). The C-5 isobutyl group is located in S1 with the *n*-butyl urea extending into the S3 subpocket in a way similar to the occupation of this site by compound **1** (Figure 1). The distal nitrogen of the urea group forms a H-bond with the hydroxyl group of Thr²³² and the carbonyl of the urea is H-bonded to the N–H of the same residue. The urea *n*-butyl group of **32** adopts an S-cis amide

bond conformation in order to extend into the narrow S3 subpocket.

B. Optimization of Mode B Inhibitors. Iminohydantoin **31** and **32** represented two completely different directions for BACE-1 inhibitor development. At the time, mode A inhibitor **31** had the best BACE-1 potency with an unoptimized occupation of the S1 and S1' sites in addition to the newly discovered “A site”, all of which would be attractive sources for BACE-1 potency improvement. On the other hand, mode B inhibitor **32**, despite its weaker BACE-1 potency, also offered obvious ways for further optimization. For example, optimization of the S1 hydrophobic interaction, occupation of the S2' binding pocket extending from the C-5 methyl group, and stabilization of the energetically disfavored S-cis amide conformation³⁹ of the distal urea group were among the most attractive directions. However, the most prominent difference between **31** and **32** was the requirement of the number of H-bonding donors on the urea functionality for BACE-1 potency. While it seemed clear for **31** to require two H-bonding donors on the urea at the “A-site” to achieve the μM affinity (Figure 9), the X-ray structure of **32** clearly suggested only one at the entrance to the S3 subpocket

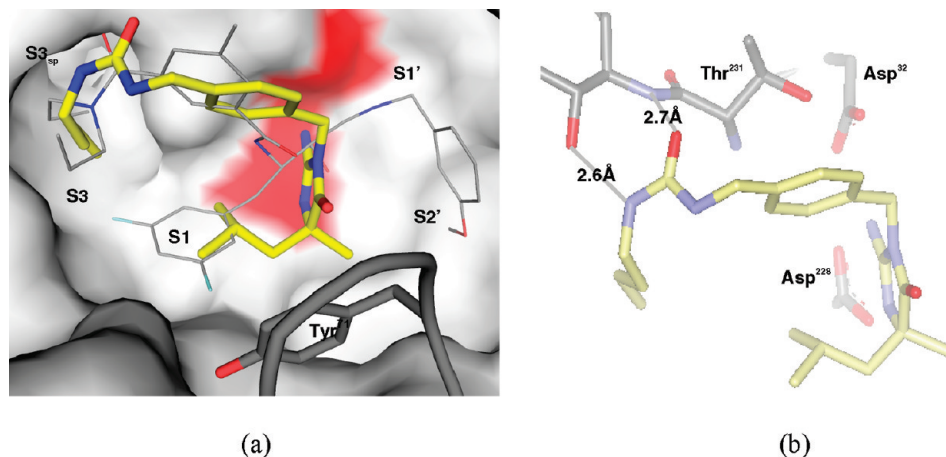


Figure 10. (a) Superimposed X-ray conformation of HEA inhibitor **1** (gray line) and iminohydantoin **32** (yellow). (b) **32** is a mode B inhibitor with its urea reaching into the S3_{sp} in a fashion similar to **1**. The distal amide bond of the urea has an S-cis conformation.

(Figure 10). Furthermore, compound **1** (gray line in Figure 10a), which occupies the S3_{sp} in an almost identical manner with **31**, even suggested that none of the hydrogen bonding donors were absolutely necessary at S3_{sp} in order to retain high BACE-1 affinity. We might be able to obtain high affinity iminohydantoin BACE-1 inhibitors based on the mode B inhibitor **32** without a need to add a single H-bonding donor, a feature that is not possible from the mode A inhibitors due to the structural requirements of the “A-site”. We therefore focused on the SAR development of the mode B inhibitors based on iminohydantoin **32**.

Replacement of the isobutyl group in **32** (5-isobutyl-5-methyl) with a cyclohexylmethyl (**33**) (5-cyclohexylmethyl-5-methyl) lowered the K_i to 5 μ M, while a benzyl group replacement (**34**) (5-benzyl-5-methyl) of the isobutyl decreased BACE-1 potency. Iminohydantoin **35** (5,5-dicyclohexylmethyl) did not further improve the binding affinity relative to **33** (5-cyclohexylmethyl-5-methyl) despite the confirmation by an enzyme cocrystal X-ray structure of **35** as a mode B inhibitor with one cyclohexylmethyl residing in S1 and the other extending into the S2' pocket (not shown). Iminohydantoin **36** (5-isobutyl-5-phenethyl), as a result of replacement of the methyl group in **32** (5-isobutyl-5-methyl) with a phenethyl, did not improve the BACE-1 IC₅₀ (78 vs 50 μ M, respectively). However, inhibitor **37** (5-isobutyl-5-cyclohexylethyl) restored the level of BACE-1 IC₅₀ (5 μ M) comparable to **33** (5-cyclohexylmethyl-5-Me). Interestingly, if the cyclohexylethyl group in racemic **37** (5-isobutyl-5-cyclohexylethyl) were to reside in the S2' pocket, this would represent an IC₅₀ improvement of 26-fold in comparison with **32** (5-isobutyl-5-methyl), a fact later established by X-ray crystallography. Combination of the 5-cyclohexylmethyl and 5-cyclohexylethyl groups afforded compound **38** with further improved BACE-1 potency (IC₅₀ 350 nM). With the confirmation of the productive occupation of the S2' site with the cyclohexylethyl, such as in **38**, we then attempted the stabilization of the bioactive S-cis amide conformation through a cyclic urea. This effort led to iminohydantoin **39** with a BACE-1 IC₅₀ of 27 nM as the 5-(*R*) enantiomer. The 3000-fold IC₅₀ improvement from the early lead **32** seems to be additive in free energy contributions from all three major components, i.e., 16-fold from S1 optimization (**32** to **33**), 26 fold from S2' occupancy (**32** to **37**), and 13-fold from stabilization of high energy bioactive conformation (**38** to **39**).

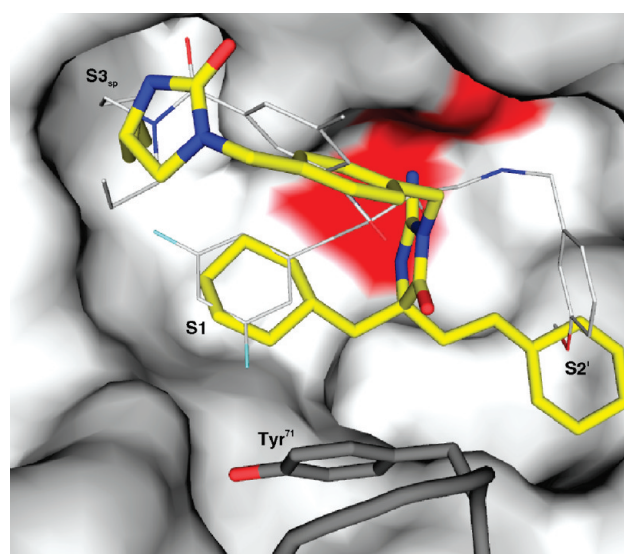


Figure 11. Iminohydantoin **39** (yellow) occupies the S1, S2' and S3_{sp} binding pockets with an open flap position (grey tube). Superimposed **1** (light grey line) is also shown.

X-ray crystallography showed clear electron density of **39** inside the BACE-1 substrate binding pocket. The occupation of the S2' binding pocket of **39** prevented the flap from closing (grey back-bone tube representation in Figure 11) as exemplified by lack of electron density for the complete flap region. By virtue of its BACE-1 potency, iminohydantoin **39** unequivocally established the validity of the iminoheterocyclic BACE inhibitor design and resolved questions regarding the intrinsic potency of the iminohydantoin core in comparison with the well established HEA motif. It further established that a closed flap position is not required to obtain high BACE-1 binding affinity. Unlike the HEA class of peptidomimetic BACE inhibitors that have a peptidic linear assembly of multiple groups to pick-up interactions with the enzyme, the iminoheterocycle core is more compact with three-dimensional trajectories to place these groups into prime and nonprime pockets. Combined with the unique interactions of the amidine group with the catalytic diad, the iminoheterocycle offered new strategies for inhibitor development.

C. Strategy for Inhibitor Development. Iminohydantoin **39** has a relatively high molecular weight (545 Da), a clogP of

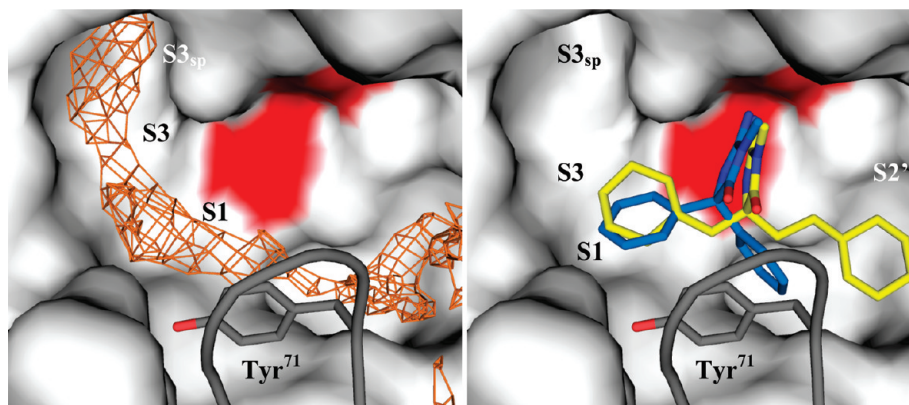


Figure 12. (a) Available hydrophobic surface of the BACE-1 substrate binding pocket with **40** stretches from S2', S1, S3 to S3_{sp} (brown wire mesh), prompting an S1–S3 inhibitor development strategy. The flap is in an opened position. (b) Iminohydantoin **40** (yellow) and **41** (blue) bound in the active site of BACE-1. Note the “tilted” position associated with **41** core, which caused a divergent SAR between these two leads. The open flap with the phenol of Tyr⁷¹ is also shown.

7.5, a ligand efficiency⁴⁰ of 0.25, a large cell IC₅₀ shift (> 30×), and rather modest rat oral exposure (rat AUC of 0.6 μM·h at 10 mg/kg po).⁴¹ Its molecular properties are not considered to be ideal for a CNS drug. However, upon inspection of available X-ray crystal structures of **32** to **39** bound to BACE-1, it became clear that the common N-3 benzyl group serves only as a rigid spacer to place an alkyl group into the S3 subpocket. Moreover, the S1 binding pocket has a proximity to the S3 and S3_{sp} pockets, which are all hydrophobic in nature. A continuous hydrophobic surface (brown wire mesh in Figure 12a) stretches from S1 to S3 and extending to S3_{sp}, presenting attractive opportunities for an alternative route to occupy the S3 binding pockets with a group extending from the S1 moiety (S1 to S3 strategy). This approach would be far more efficient, affording the possibility of obtaining BACE-1 inhibitors with much lower molecular weight.⁴²

To launch the S1 to S3 approach, it was necessary to truncate the S3 binding group attached to N3 of inhibitor **39**. Recognizing the importance of maintaining the appropriate basicity of the iminohydantoin core, as indicated by the lack of BACE-1 affinity of type II iminohydantoin such as **11**, we decided to retain the methyl substitution at N3. We were pleased to find that iminohydantoin **40**, despite a reduction of a near-half of the molecular weight, showed a BACE-1 IC₅₀ of 600 nM, corresponding to a ligand efficiency of 0.36. This compound also had a much reduced cell IC₅₀ shift (4×).

X-ray crystallography revealed that iminohydantoin **40** does not undergo any major conformational shift resulting from the truncation of the N3 group (Figure 12), with the ligand electron density almost identical with the corresponding substructure in **39** (Figure 11). Although compound **40** had a modest oral rat PK profile (AUC_{0–6h} = 1 μM·h at 10 mg/kg po), it was brain penetrant with a 6 h *b/p* ratio of 1 and a brain concentration at 6 h of over 100 nM. It was the first small molecule iminohydantoin BACE inhibitor that we had identified with such a promising overall profile.

Emboldened by this finding, we next focused on extensive SAR explorations aimed at modification/replacement of the 5,5-substituents of **40** in an effort to improve the BACE-1 affinity through optimization of the occupation of the interconnected binding pockets S1, S3, and S3_{sp}. As a result, compound **41** was soon identified with a BACE-1 IC₅₀ of

Table 3. Compound Profile of the Truncated Iminohydantoin **40** and **41**^a

	40	41
MW; cLogP	319; cLogP = 5.4	265; cLogP = 1.9
ligand efficiency	0.36	0.37
BACE-1 IC ₅₀	605 nM	7100
HEK293 cell IC ₅₀	2600 nM	12000
rat PK (<i>b/p</i> ratio) ^b	1 μM·h; (<i>b/p</i> = 0.9)	5 μM·h; (<i>b/p</i> = 1.8)
cath D K _i	740 nM	38% @ 50 μM

^a Each IC₅₀ value is an average of three determinations and the standard errors for all IC₅₀ determinations are less than 10%. ^b Data from pooled samples from two mice in cassette accelerated rapid rat protocol with an oral dose at 10 mg/kg, brain plasma ratio obtained at 6 h time point.

7 μM. Despite its weaker BACE-1 potency in comparison with **40**, it had a substantially improved selectivity against cathepsin D,⁴³ minimum HEK293 cell IC₅₀ shift (< 2 fold), and an improved rat pharmacokinetic profile with a brain plasma ratio of 1.8 (Table 3). The iminohydantoin core of **41** is tilted from that in **40** in order for the BACE-1 enzyme to accommodate the C-5 phenyl group (Figure 12). This small conformational change of **41** related to **40** caused divergence of the iminohydantoin C-5 position SAR, which rendered a simple hybridization of the C5-groups among these two leads unsuccessful. Interestingly, the iminogroups from both X-ray structures are superimposable despite the positional changes of the remainder of the two inhibitors.

With a molecular weight around 300 Da, two hydrogen bond donors, two hydrogen bond acceptors and high ligand efficiency, iminohydantoin **40** and **41** offered excellent starting points for further development of CNS penetrant aspartyl protease inhibitors. Further optimization of these aspartyl protease inhibitors through S3, S3_{sp}, and S2' sites optimization will be subjects of future publications. After a patent covering our discovery effort on these novel BACE-1 inhibitors presented in this manuscript was published,⁴⁴

two independent research groups reported similar imino-hydantoin and iminopyrimidinone BACE-1 inhibitor designs, the first starting from acyclic or cyclic acylguanidine as high-throughput screening hits,⁴⁵ the second from a fragment-based screening effort similar to what is reported here.⁴⁶ The full establishment of these CNS penetrant BACE-1 inhibitors sparked an effort to obtain drugs with potential to halt or even reverse AD. Further efforts from our laboratories in this area will be the subject of future publications.

Conclusion

Novel amidine containing heterocycles were designed to mimic the interaction pattern between BACE-1 catalytic diad and a weak NMR screening hit (**3**), as revealed by X-ray crystallography. Special attention was paid to maintaining the appropriate basicity and limiting the number of H-bonding donor of these scaffolds. Initial inhibitor designs were computationally evaluated and were predicted to bind to the BACE-1 catalytic site, reproducing the binding interactions with the enzyme revealed by the early lead. Two binding modes (A and B) were identified with these initial imino-heterocycle BACE inhibitors as revealed by X-ray crystallography. The iminohydantoin core in one binding mode is flipped 180° in relation to the other and each core forms a bidentate interaction with one of the two catalytic aspartates respectively. The detailed amidine–aspartate interactions are highly conserved among the two binding modes with a near C2 symmetry present in the superimposed diad–inhibitor conformations. The exocyclic imino group serves as a replacement of the water in the apo protein between the two catalytic aspartic acids. Through a combination of high throughput synthesis and extensive use of structural-based drug design tools, highly potent iminohydantoin BACE-1 inhibitors have been obtained, validating the molecular design as aspartyl protease catalytic site inhibitors. Throughout the endeavor, emphasis on optimum pharmacokinetic profile and brain penetration, highlighted by restricting molecular weight and minimizing the number of hydrogen bond donors outweighed a linear pursuit of binding affinity. Brain penetrant small molecule BACE inhibitors with high ligand efficiencies have been discovered, paving the way for highly potent, selective, and in vivo efficacious BACE inhibitors.

The iminoheterocycles as an established druggable motif with high bioavailability and CNS penetration will likely find applications beyond BACE-1 inhibition in areas of other aspartyl proteases such as renin and plasmepsins. In addition, there are additional enzyme targets with biochemical mechanisms involving carboxylic acid side chains against which the new design can be applied.⁴⁷ Finally, iminohydantoin should also serve as a viable pharmacophore isostere replacement of amidines and guanidines, both have difficulty to achieve oral bioavailability in a number of drug development programs.

Experimental Section

NMR Chemical Shift Perturbation. The details of the NMR experimental procedures are described in the companion paper (ref 24).⁴⁸

Molecular Modeling. Molecular Docking. All water molecules and the ligand were deleted and hydrogen atoms were added using Maestro 5.1. A Glide grid was computed for the protein structure (Impact v1.8 for 10, subsequently Impact v 2.7)⁴⁹ with an inner box region (the ligand midpoint remains within this box during docking) of 16 Å and outer box region of

36 Å. The grid midpoint was defined by the centroid of one of the ligands in the data set. Default settings were used for the docking runs and 10 poses were reported.

Hydrophobic Maps. The sitemap program in Maestro 5.1 was used to calculate hydrophobic maps using default settings and a bounding box of 6 Å around the ligand of the crystal structures, after addition of hydrogen atoms.

Relative Energies. The relative energies were calculated with Jaguar v. 5.5 (ref 49) using the B3LYP hybrid density functional and for geometry optimizations the 6-31G**+ basis set. Single point energies of tautomers (a) and (b) were calculated based on the optimized geometries (B3LYP/CC-PVTZ(-F)++) applying the Poisson–Boltzmann aqueous solvation model. Gas phase single point energies (B3LYP/CC-PVTZ(-F)++) of the optimized S-cis and S-trans ureas.

X-ray Crystallography. X-ray crystal structure of the complex of BACE-1 and compound **3** was obtained by co-crystallization. BACE-1 (16 mg/mL, 150 mM NaCl and 20 mM Hepes at pH 7.5) was complexed with 1 mM of compound **2** and mixed 1:1 with reservoir (15% PEG3350 and 0.2 M Na/K tartrate). The hanging drops were incubated at 4 °C for several weeks until diffraction quality crystals grew. Crystals were cryoprotected (15% PEG3350, 0.2 M Na/K tartrate, and 15% PEG400) and flash frozen prior to data collection. Data was collected with a Raxis IV detector using a Raxis RU-H2R generator. The final data set was 99% complete to 1.8 Å resolution with an *R* merge of 5.7%. Crystal structures of further complexes were obtained by soaking the cocrystals of compound **2** in a solution (20% PEG 3350, 0.1 M Na/K tartrate, and 15% PEG400) containing the new compound for approximately 24 h. The structures were refined with CNX (Accelrys).

Protease in Vitro Assays. The Europium/QSY-7-labeled BACE-1 FRET peptide substrate (QSY7-EISEVNLDAEFC-Eu-amide) contains the QSY7:europium donor:acceptor pair for use in time-resolved FRET assays. Mature BACE-1 (autoBACE-1) comprised of amino acids 41–454 was used in all in vitro BACE-1 enzymatic assays. Soluble mature BACE-2 comprised of amino acids 63–389, was used in all in vitro BACE-2 enzymatic assays. Purified human liver cathepsin D (Athens Research) was used for in vitro counterscreen assay with its proteolytic activity measured using the FRET peptide substrate Mca-Gly-Lys-Pro-Ile-Leu-Phe-Phe-Arg-Leu-Lys(Dnp)-D-Arg-NH₂ (Bachem).

Determination of BACE-1 and BACE-2 IC₅₀s. A time-resolved FRET assay was used as previously described.⁵⁰

Determinations of Inhibitor BACE-1 K_i. Inhibitors, prepared at 3× the desired final concentration in 1× BACE assay buffer (20 mM sodium acetate pH 5.0, 10% glycerol, 0.1% Brij-35) supplemented with 7.5% DMSO were preincubated with an equal volume of autoBACE-1 or autoBACE-2 enzyme diluted in 1× BACE assay buffer (final enzyme concentration 1 nM) in black 384-well NUNC plates for 30 min at 30 °C. The assay was initiated by addition of an equal volume of the QSY7-EISEVNLDAEFC-Eu-amide substrate (200 nM final concentration, *K_m* = 8 μM for autoBACE-1 and 4 μM for autoBACE-2) prepared in 1× BACE assay buffer supplemented with 7.5% DMSO and incubated for 90 min at 30 °C. DMSO was present at 5% final concentration in the assay. Following laser excitation of sample wells at 320 nm, the fluorescence signal at 620 nm was collected for 400 ms following a 50 μs delay on a RUBYstar HTRF plate reader (BMG Labtechnologies). Raw RFU data was normalized to maximum (1.0 nM BACE/DMSO) and minimum (no enzyme/DMSO) RFU values. IC₅₀s were determined by non-linear regression analysis (sigmoidal dose response, variable slope) of percent inhibition data with minimum and maximum values set to 0 and 100%, respectively. Similar IC₅₀s were obtained when using raw RFU data. The *K_i* values were calculated from the IC₅₀ using the Cheng–Prusoff equation (BACE-1 *K_m* = 8 μM and BACE-2 *K_m* = 4 μM for the QSY7-APP^{swc}-Eu peptide substrate).

Determination of Cathepsin D IC₅₀ and K_i. Human cathepsin D (CatD, 0.063 nM) was preincubated with compounds diluted in 1 × CatD assay buffer (100 mM sodium acetate pH 5.0, 0.02% Brij-35, 1.5% DMSO) for 30 min at 37 °C in 384-well plates followed by addition of the Mca-Gly-Lys-Pro-Ile-Leu-Phe-Phe-Arg-Leu-Lys(Dnp)-D-Arg-NH₂ substrate (2.5 μM final concentration assay buffer, K_m = 4 μM). DMSO was present at 1% final concentration in the assay. Following a 45 min incubation at 37 °C, plates were read on a Molecular Devices Flex Station set at 328 nm excitation and 393 nm emission. IC₅₀ and K_i values were determined as for BACE assays.

Determination of IC_{50s} for Aβ₄₀ in HEK293-APP^{swe/lon} Cells. HEK-293 cells were stably transfected with human APP containing the Swedish and London mutations (HEK293-APP^{swe/lon} cells). These mutations result in increased amyloidogenic processing of APP and increased secretion of Aβ₄₀ and Aβ₄₂. HEK293-APP^{swe/lon} cells were maintained in Dulbecco's modified Eagle's medium (GIBCO) supplemented with 10% fetal bovine serum (GIBCO), 1% penicillin–streptomycin, and 250 μg/mL hygromycin B (GIBCO) (complete media). Cells were plated at 25000 cells/well in 96-well culture dishes 3 days prior to the assay. On the day of the assay, culture media was removed from duplicate wells and replaced with 100 μL of fresh complete media containing vehicle (0.2% DMSO) or increasing concentrations of inhibitors (10⁻⁶ M–10⁻¹¹ M). Cells were incubated for 4 h at 37 °C/5% CO₂ followed by measurement of secreted Aβ_{1–40} using an electrochemiluminescence-based (ECL) sandwich ELISA. Briefly, 15 μL of cell culture media from four 96-well plates were transferred to one 384-well avidin-coated MSD plate (Mesoscale Discovery) using an automated microplate pipetting system (Precision 2000, Biotek Instruments). For Aβ_{1–40}, 15 μL of 2 × Aβ₄₀-ELISA buffer (2% BSA, 2% Tween-20, 0.3 M NaCl, 0.1 M HEPES, pH 7.5) supplemented with 0.25 μg/mL biotin-WO₂⁷ capture antibody and 0.125 μg/mL Ruthenium-G2–10 detection antibody was added to each well. ELISA plates were then incubated overnight at 4 °C and 10 μL of 4 × MSD read buffer T/well (Mesoscale Diagnostics) was added immediately before reading on a Sector Imager 6000 plate reader (Mesoscale Diagnostics). IC_{50s} were determined from best fit nonlinear regression analysis of the raw ECL data using an equation for a sigmoidal dose response (variable slope). Curve minimum values were fixed to the ECL counts measured in the presence of 10 μM of a reference BACE-1 inhibitor (BACE-1 K_i = 9 nM) and were determined for every set of four 96-well plates.

Synthesis. All reagents were obtained from commercial sources unless noted otherwise. All NMR data were collected on 400 MHz NMR spectrometers unless otherwise indicated. The chemical shifts are expressed as ppm downfield from tetramethylsilane or as relative ppm from designated reference peaks. The purity of final compounds was analyzed on two independent reverse phase HPLC systems with different gradient. LC-electrospray-mass spectroscopy with a C-18 column using a gradient of 5% to 95% MeCN in water as the mobile phase was used to determine the molecular mass and retention time. The purity of the samples was assessed using a mass detector and a UV detector at 254 nm. An additional analytical reverse phase HPLC system was used to assess the purity of final compounds using a UV detector monitored at both 219 and 254 nm and an ELSD detector. All compounds have purity greater than 95%.

Synthesis of 3-(3-Chloro-benzyl)-5,5-dimethyl-2-iminohydantoin (10). 2-Amino-*N*-(3-chlorobenzyl)-2-methylpropanamide. A mixture of *N*-Boc-α-methylalanine (3.0 g, 14.8 mmol), EDCI (2.8 g, 14.8 mmol), HOAt (2.1 g, 14.8 mmol), and DIEA (2.6 mL, 14.8 mmol) in 36 mL of DCM was stirred at rt for 15 min before 3-chlorobenzylamine was added and the reaction mixture stirred at rt overnight. The crude mixture was purified on a silica gel column using 30% EtOAc in DCM containing 0.7% 2 M NH₃ in MeOH solution and DCM as an eluent system. The resulting

product was treated with 4 M HCl in dioxane and neutralized with 1N NaOH to give 2-amino-*N*-(3-chlorobenzyl)-2-methylpropanamide (1.9 g, 56.7% yield).

¹H NMR (CD₃OD): δ 7.27–7.15 (m, 4H), 4.31 (s, 2H), 1.29 (s, 6H).

3-(3-Chlorobenzyl)-5,5-dimethyl-2-thiohydantoin. Thiophosgene (0.7 mL, 9.2 mmol) in 10 mL of DCM was added dropwise to a solution of 2-amino-*N*-(3-chlorobenzyl)-2-methylpropanamide (1.9 g, 8.3 mmol) in 35 mL of DCM at 0 °C under nitrogen, followed by slow addition of TEA (1.68 mL, 12.0 mmol) in 5 mL of DCM. The reaction solution was stirred at 0 °C for 30 min, then quenched with aqueous sodium bicarbonate and extracted with DCM. The crude mixture was purified on a silica gel column with DCM/hexane (4:1) containing 0.4% 2 M NH₃ in MeOH to give 3-(3-chlorobenzyl)-5,5-dimethyl-2-thiohydantoin (1.7 g, 77.2% yield).

¹H NMR (CD₃OD): δ 7.33 (br s, 1H), 7.25–7.22 (m, 3H), 4.90 (s, 2H), 1.33 (s, 6H).

3-(3-Chloro-benzyl)-5,5-dimethyl-2-iminohydantoin (10). A solution of 3-(3-chlorobenzyl)-5,5-dimethyl-2-thiohydantoin (0.2 g, 0.74 mmol), 70% aqueous *t*-butyl hydroperoxide (1.2 mL, 10.1 mmol) and 30% ammonium hydroxide (4.1 mL) in 12 mL of MeOH was stirred at rt for 42 h. After removal of volatiles, the crude reaction mixture was purified on a C18 column to give **10** as a white solid (0.1 g, 54.4% yield).

¹H NMR (DMSO-*d*₆): δ 7.42–7.37 (m, 3H), 7.19 (m, 1H), 4.79 (m, 2H), 1.33 (s, 6H). ES-LCMS: *m/z* = 252 [M + H]⁺.

5-Methyl-5-isopropyl-1-(*m*-chlorobenzyl)-2-iminohydantoin (21). 5-Methyl-5-isopropyl-1-(*m*-chlorobenzyl)-2-thio-4-*N*-benzyliminohydantoin. To a solution of 3-chlorophenethyl amine hydrochloride (1.1 g, 5.73 mmol) in anhydrous CH₃OH (15 mL) was added KSCN (0.56 g, 5.73 mmol). The reaction mixture was heated to 60 °C for 1 h. The suspension was filtered and the filtrate was added to 4-methyl-2-pentanone (0.72 mL, 5.73 mmol) and benzyl isocyanide (0.77 mL, 6.3 mmol). The mixture was stirred overnight before the solution was concentrated and the residue was purified via flash chromatography eluting with 0–100% EtOAc in hexane to yield 0.28 g of desired product.

5-Methyl-5-isopropyl-1-(*m*-chlorobenzyl)-2-thiohydantoin. A solution of 40% conc HCl in ethanol was added to 5-methyl-5-isopropyl-1-(*m*-chlorobenzyl)-2-thio-4-*N*-benzyliminohydantoin and the solution was heated in a microwave at 160 °C for 30 min. The solution was concentrated and purified via reverse phase preparative HPLC eluting with a CH₃CN/H₂O gradient to afford 5-methyl-5-isopropyl-1-(*m*-chlorobenzyl)-2-thiohydantoin.

5-Methyl-5-isopropyl-1-*m*-chlorobenzyl-2-iminohydantoin (21). A procedure similar to the step leading to compound **10** was used.

¹H NMR(CD₃OD): δ 8.1 (br, 1H), 7.35 (s, 1H), 7.25 (m, 3H), 3.6 (m, 1H), 3.4 (m, 1H), 3.0 (m, 1H), 2.8 (m, 1H), 1.75 (m, 1H), 1.6 (m, 1H), 1.35 (m, 1H), 1.2 (s, 3H), 0.8 (m, 6H). ES-LCMS: *m/z* = 308.1 [M + H]⁺.

3-(3-Chlorobenzyl)-5-isobutyl-5-methyl-2-iminohydantoin (23). 3-(3-Chlorobenzyl)-5-isobutyl-5-methyl-2-thiohydantoin(15). The reaction solution of α-methylleucine methyl ester (150 mg, 1.16 mmol) and 3-chlorobenzyl isothiocyanate (22.4 mg, 1.22 mmol) in 7 mL of DCM was stirred at rt overnight. The crude was purified on a silica gel column to give the desired product.

¹H NMR (CD₃OD): δ 7.39 (m, 1H), 7.33–7.30 (m, 1H), 7.25–7.22 (m, 1H), 4.99–4.83 (dd, 2H), 1.73–1.67 (m, 1H), 1.60–1.55 (m, 1H), 1.29 (s, 3H), 0.82–0.80 (d, 3H), 0.62–0.60 (d, 3H).

3-(3-Chlorobenzyl)-5-isobutyl-5-methyl-2-iminohydantoin (23). A procedure similar to the step leading to compound **10** was used.

¹H NMR (CD₃OD): δ 7.34–7.30 (m, 3H), 7.27–7.24 (m, 1H), 4.90–4.78 (dd, 2H), 1.73–1.70 (d, 2H), 1.51–1.36 (m, 1H), 1.41 (s, 3H), 0.84–0.83 (d, 3H), 0.66–0.65 (d, 3H). ES-LCMS: *m/z* = 294 [M + H]⁺.

5,5-Dimethyl-1-(*m*-chlorophenethyl)-2-iminohydantoin (24). A procedure similar to the step leading to compound **10** was used.

^1H NMR (CD_3OD): δ 7.34 (s, 1H), 7.28–7.19 (m, 3H), 3.61–3.54 (br t, 2H), 2.93–2.89 (t, 2H), 1.30–1.22 (br s, 6H). ES-LCMS: $m/z = [\text{M} + \text{H}]^+$.

3-[4-[3-(4-Cyanophenyl)ureidomethyl]benzyl]-5-isobutyl-5-methyl-2-iminothiohydantoin (31). Methyl 2-Isothiocyanato-2,4-dimethylpentanoate (**13**). A solution of 1,1'-thiocarbonyldi-2(1*H*)-pyridone (0.7 g, 3.0 mmol) in 8 mL of DCM was added dropwise to a solution of α -methylleucine methyl ester (**12**, 0.43 g, 2.7 mmol) in 7 mL of DCM. The reaction solution was stirred at rt overnight, diluted with DCM, washed with 1N HCl and brine, and dried with anhydrous Na_2SO_4 to give **13** as a crude product, which was used without further purification.

^1H NMR (CDCl_3): δ 3.74 (s, 3H), 1.86–1.81 (m, 1H), 1.79–1.70 (m, 1H), 1.68–1.63 (m, 1H), 1.55 (s, 3H), 0.93–0.91 (d, 3H), 0.83–0.81 (d, 3H).

3-(4-Aminomethylbenzyl)-5-isobutyl-5-methyl-2-thiohydantoin. A solution of 4-(*N*-Boc-aminomethyl)benzylamine (2.4 g, 10.2 mmol) in 10 mL of DCM was added dropwise to a solution of the crude **13** in 45 mL of DCM. The reaction solution was stirred at rt overnight, and purified on a silica gel column with EtOAc/hexane to give corresponding thiohydantoin which was deprotected with 50% TFA in DCM to give 3-(4-aminomethylbenzyl)-5-isobutyl-5-methyl-2-thiohydantoin after removal of solvents. This was used for next step without further purification.

^1H NMR (CDCl_3): δ 7.37–7.35 (d, 2H), 7.19 (s, 1H), 7.18–7.16 (d, 2H), 4.93–4.92 (m, 2H), 4.24–4.23 (m, 3H), 1.73–1.45 (m, 3H), 1.40 (s, 9H), 1.34 (s, 3H), 0.83–0.82 (d, 3H), 0.69–0.68 (d, 3H).

3-[4-[3-(4-Cyanophenyl)ureido]methyl]benzyl-5-isobutyl-5-methyl-2-thiohydantoin. 3-(4-Aminomethylbenzyl)-5-isobutyl-5-methyl-2-thiohydantoin was treated with 2 equiv of 4-cyanophenyl isocyanate (72 mg, 0.25 mmol) in 5 mL of DCM at rt overnight. Trisamine resin (6 equiv) was added to trap excess of the isocyanate. The filtrate was concentrated in vacuum to give 3-[4-[3-(4-cyanophenyl)ureido]methyl]benzyl-5-isobutyl-5-methyl-2-thiohydantoin, which was used without further purification.

3-[4-[3-(4-Cyano-phenyl)ureidomethyl]benzyl]-5-isobutyl-5-methyl-2-iminothiohydantoin (31). A procedure similar to the step leading to compound **10** was used.

^1H NMR (CD_3OD): δ 7.55 (d, 2H), 7.47 (d, 2H), 7.29 (d, 2H), 7.21 (d, 2H), 4.83–4.79 (m, 2H), 4.30 (s, 2H), 1.68–1.67 (d, 2H), 1.45–1.42 (m, 1H), 1.36 (s, 3H), 0.79–0.78 (d, 3H), 0.63–0.61 (d, 3H). ES-LCMS: $m/z = 433 [\text{M} + \text{H}]^+$.

Parallel Synthesis Procedure for Iminothiohydantoin Such as 32 and 34. Isothiocyanate **13** in DCM was loaded into a deep 96-well plate followed by treatment of 1.1 equiv 96 primary amines in DCM. The subsequent reaction mixtures were treated with sulfonic acid resin to remove the excess amine. After filtration, the thiourea solutions were concentrated and the residues were treated with 5:1 v/v ratio of 7 M NH_3 in methanol and 70% aqueous solution of tBuOOH. After the sealed plate was agitated overnight, the solvent was evaporated, the residues redissolved in THF and the solutions were treated with sulfonic acid resin to scavenge the basic product. After wash and release of the products with NH_3 in methanol from the solid support, the desired iminothiohydantoin were obtained, in most cases, without the need for further purification.

3-[(3-Butylureidomethyl)benzyl]-5-isobutyl-5-methyl-2-iminothiohydantoin (32). ES-LCMS: $m/z = 388 [\text{M} + \text{H}]^+$.

3-[(3-Butylureido)methyl]benzyl-5-benzyl-5-cyclohexylmethyl-2-iminothiohydantoin (34). ES-LCMS: $m/z = 422 [\text{M} + \text{H}]^+$.

3-[(3-Butylureidomethyl)benzyl]-5-cyclohexylmethyl-5-methyl-2-iminothiohydantoin (33). A procedure similar to the step leading to compound **10** was used.

^1H NMR (CD_3OD): δ 7.24 (s, 2H), 4.84–4.66 (m, 2H), 4.24 (s, 2H), 3.09–3.05 (t, 2H), 1.70–1.25 (m, 11H), 1.31 (s, 3H), 1.08–0.69 (m, 6H), 0.90–0.86 (t, 3H). ES-LCMS: $m/z = 428 [\text{M} + \text{H}]^+$.

3-[(3-Butylureido)methyl]benzyl-5,5-dicyclohexylmethyl-2-iminothiohydantoin (35). A procedure similar to the step leading to compound **10** was used.

^1H NMR (CD_3OD): δ 7.31–7.25 (m, 4H), 4.87–4.73 (m, 2H), 4.25 (s, 2H), 3.09–3.05 (t, 2H), 1.70–1.24 (m, 18H), 1.10–0.75 (m, 12H), 0.90–0.86 (t, 3H). ES-LCMS: $m/z = 510 [\text{M} + \text{H}]^+$.

3-[(3-Butylureido)methyl]benzyl-5-isobutyl-5-phenethyl-2-iminothiohydantoin (36). A procedure similar to the step leading to compound **10** was used.

^1H NMR (CD_3OD): δ 7.34–7.22 (m, 6H), 7.18–7.14 (m, 1H), 7.09–7.05 (d, 2H), 4.74 (s, 2H), 4.27 (s, 2H), 3.11–3.08 (t, 2H), 2.56–2.48 (m, 1H), 2.33–2.25 (m, 1H), 2.13–1.96 (s, 2H), 1.80–1.68 (m, 2H), 1.51–1.28 (m, 5H), 0.93–0.89 (t, 3H), 0.87–0.85 (d, 3H), 0.72–0.70 (d, 3H). ES-LCMS: $m/z = 478 [\text{M} + \text{H}]^+$.

3-[(3-Butylureidomethyl)benzyl]-5-cyclohexylethyl-5-isobutyl-2-iminothiohydantoin (37). A procedure similar to the step leading to compound **10** was used.

^1H NMR (CD_3OD): δ 7.28–7.23 (m, 4H), 4.87–4.23 (m, 2H), 4.25 (s, 2H), 3.09–3.03 (t, 2H), 1.77–1.51 (m, 9H), 1.48–0.94 (m, 10H), 0.90–0.86 (t, 3H), 0.84–0.82 (d, 3H), 0.79–0.65 (m, 3H), 0.70–0.69 (d, 3H). ES-LCMS: $m/z = 484 [\text{M} + \text{H}]^+$.

3-[(3-Butylureido)methyl]benzyl-5-cyclohexylethyl-5-cyclohexylmethyl-2-iminothiohydantoin (38). A procedure similar to the step leading to compound **10** was used.

^1H NMR (CD_3OD): δ 7.32–7.24 (m, 4H), 4.89–4.24 (m, 2H), 4.25 (s, 2H), 3.09–3.05 (t, 2H), 1.83–0.75 (m, 32H), 0.90–0.86 (t, 3H). ES-LCMS: $m/z = 524 [\text{M} + \text{H}]^+$.

(*R*)-5-(2-Cyclohexylethyl)-5-(cyclohexylmethyl)-3-[4-(2-oxo-4(*S*)-propylimidazolidin-1-yl)methyl]benzyl-2-iminothiohydantoin (39). (*S*)-2-Amino-4-cyclohexylbutanoic Acid. (*S*)-Homophenylalanine (100 g, 558 mmol) in 1000 mL of MeOH, 200 mL of H_2O , and 100 mL of concentrated HCl was hydrogenated at 60 psi using Pt (5% on carbon) and Rh (5% on carbon with 50% water) as catalysts to give the titled compound, which was used for next step without further purification.

^1H NMR (CD_3OD): δ 3.96–3.92 (t, 1H), 2.00–1.82 (m, 2H), 1.80–1.63 (m, 5H), 1.45–1.15 (m, 6H), 1.05–0.85 (m, 2H).

(2*S*,4*S*)-Benzyl 4-(2-cyclohexylethyl)-5-oxo-2-phenyloxazolidine-3-carboxylate. A solution of Cbz-OSu (139 g, 558 mmol) in 300 mL of dioxane was added to a suspension of (*S*)-2-amino-4-cyclohexylbutanoic acid in 500 mL of dioxane, 500 mL of H_2O , and 93 mL of TEA (667 mmol). The reaction mixture was stirred at rt overnight and then poured into water and extracted with DCM. The organic phase was washed with 1N HCl, water, brine, and then dried over anhydrous MgSO_4 to give 110 g (345 mmol) of the Cbz protected product as a crude product which was used without further purification. Thionyl chloride (25.5 mL, 349 mmol) was added dropwise to a solution of this Cbz protected product and benzaldehyde dimethylacetal (2.4 g, 345 mmol) in 600 mL of anhydrous THF at 4 °C under N_2 protection. After stirring for 10 min, anhydrous ZnCl_2 (48 g, 352 mmol) was added slowly. The reaction mixture was stirred in an ice bath for 2 h and then placed in a freezer overnight. The reaction mixture was poured into a mixture of ice and water and extracted with ether. The organic phase was washed with aqueous sodium bicarbonate and brine, dried over anhydrous MgSO_4 , and concentrated in vacuum to give the titled compound after purification.

^1H NMR (CDCl_3): δ 7.50–7.25 (m, 10H), 6.75 (s, 1H), 5.30–5.215 (m, 2H), 4.45–4.35 (m, 1H), 1.90–1.45 (m, 7H), 1.45–1.05 (m, 6H), 0.90–0.70 (m, 2H). ES-LCMS: $m/z = 408 [\text{M} + \text{H}]^+$.

(2*S*,4*R*)-Benzyl 4-Benzyl-4-(2-cyclohexylethyl)-5-oxo-2-phenyloxazolidine-3-carboxylate. A solution of (2*S*,4*S*)-benzyl 4-(2-cyclohexylethyl)-5-oxo-2-phenyloxazolidine-3-carboxylate (2.0 g, 4.91 mmol) and benzyl bromide (0.59 mL, 4.91 mmol) in 10 mL of anhydrous THF was added slowly to LiHMDS (1 M in hexane, 5.4 mL, 5.40 mmol) in 80 mL of anhydrous THF at –42 °C. The reaction mixture was stirred at about –30 °C for 1.5 h and continuously stirred while reaction temperature rose to rt. The

reaction mixture was poured into a mixture of ice and aqueous sodium bicarbonate and extracted with ether. The organic phase was washed with brine and dried over anhydrous MgSO_4 . The crude was purified on a silica gel column eluted with EtOAc/hexane to give the titled compound (1.2 g, 49.5% yield).

$^1\text{H NMR}$ (CDCl_3), of two rotamers (1:2): δ 7.43–7.03 (m, 13H), 6.94–6.88 (m, 2H), 5.29–5.12 (d, 0.66H), 5.04–4.82 (d, 1.33H), 5.00 (s, 0.33H), 4.88 (s, 0.66H), 3.63–3.60 (d, 0.66H), 3.29–3.26 (d, 0.33H), 3.04–2.98 (m, 1H), 2.53–2.43 (m, 0.66H), 2.28–2.18 (m, 0.33H), 2.16–2.00 (m, 1H), 1.77–1.32 (m, 5H), 1.30–0.98 (m, 6H), 0.96–0.72 (m, 2H).

(R)-Methyl 2-Benzyl-2-(benzyloxycarbonylamino)-4-cyclohexylbutanoate. A solution of (2*S*,4*R*)-benzyl 4-benzyl-4-(2-cyclohexylethyl)-5-oxo-2-phenylloxazolidine-3-carboxylate (1.21 g, 2.43 mmol) and LiOMe (1N in MeOH, 3.7 mL, 3.65 mmol) in 3 mL of anhydrous THF was stirred at rt overnight, and at 55 °C for 90 min. The reaction mixture was diluted with 16 mL of EtOAc and treated with 4 mL of saturated aqueous NaHSO_3 by vigorous stirring at rt for 15 min. This resulting solid was removed by filtration. The filtrate was washed with saturated aqueous Na_2SO_3 , dried over anhydrous Na_2SO_4 , and concentrated in vacuum to give the titled compound (0.93 g, 90.3% crude yield), which was used for next step without further purification.

$^1\text{H NMR}$ (CD_3OD): δ 7.37–7.25 (m, 5H), 7.13–7.08 (m, 3H), 6.91–6.88 (m, 2H), 6.65 (s, 1H), 5.06 (s, 2H), 3.67 (s, 3H), 3.27–3.10 (m, 2H), 2.02–1.94 (m, 1H), 1.77–1.56 (m, 6H), 1.20–0.97 (m, 6H), 0.86–0.74 (m, 2H).

(R)-Methyl 2-Amino-4-cyclohexyl-2-(cyclohexylmethyl)butanoate. (R)-Methyl 2-benzyl-2-(benzyloxycarbonylamino)-4-cyclohexylbutanoate (0.93 g, 2.20 mmol) was hydrogenated according to the procedure described in synthesis of (S)-2-amino-4-cyclohexylbutanoic acid to give (R)-methyl 2-amino-4-cyclohexyl-2-(cyclohexylmethyl)butanoate after neutralization as free base (0.34 g, 98.9% yield).

$^1\text{H NMR}$ (CD_3OD) (HCl salt): δ 3.78 (s, 3H), 1.92–1.48 (m, 15H), 1.40–1.09 (m, 7H), 1.04–0.78 (m, 4H).

(R)-Methyl 4-Cyclohexyl-2-(cyclohexylmethyl)-2-isothiocyanatobutanoate. A solution of 2-amino-4-cyclohexyl-2-(cyclohexylmethyl)butanoate (0.34 g, 1.15 mmol) and 1,1'-thiocarbonyldi-2(1*H*)-pyridone (0.32 g, 1.38 mmol) in 15 mL of anhydrous THF was heated at 80 °C in a sealed tube for 1 h. The crude was purified on a silica gel column with EtOAc/hexane as eluent system to give the desired product (0.161 g, 41.2% yield).

$^1\text{H NMR}$ (CDCl_3): δ 3.75 (s, 3H), 1.92–1.78 (m, 2H), 1.76–1.49 (m, 13H), 1.49–0.78 (m, 13H).

(R)-5-(2-Cyclohexylethyl)-5-(cyclohexylmethyl)-3-[4-(2-oxo-4(*S*)-propylimidazolidin-1-yl)methyl]benzyl-2-thiohydantoin. A solution of (R)-methyl 4-cyclohexyl-2-(cyclohexylmethyl)-2-isothiocyanatobutanoate (0.161 g, 0.48 mmol), (S)-1-(4-(Boc-aminomethyl) benzyl)-4-propylimidazolidin-2-one TFA salt, and DIEA (0.17 mL, 1.00 mmol) in 12 mL of anhydrous MeCN was stirred at rt for 5 h. The crude was purified on a silica gel column with EtOAc/hexane as eluent system to give the corresponding thiohydantoin (0.11 g, 43.5%).

$^1\text{H NMR}$ (CDCl_3): δ 7.85 (s, 1H), 7.42–7.40 (d, 2H), 7.14–7.12 (d, 2H), 4.97–4.87 (m, 2H), 4.35–4.18 (m, 2H), 3.65–3.59 (m, 1H), 3.33–3.29 (m, 1H), 2.86–2.82 (m, 1H), 1.78–1.35 (m, 15H), 1.32–0.69 (m, 20H).

(R)-5-(2-Cyclohexylethyl)-5-(cyclohexylmethyl)-3-[4-(2-oxo-4(*S*)-propylimidazolidin-1-yl)methyl]benzyl-2-iminothiohydantoin (39). $^1\text{H NMR}$ (CD_3OD): δ 7.35–7.33 (d, 2H), 7.26–7.24 (d, 2H), 4.95–4.69 (m, 2H), 4.31–4.22 (m, 2H), 3.62–3.56 (m, 1H), 3.39–3.35 (m, 1H), 2.89–2.85 (m, 1H), 1.75–0.72 (m, 32H), 0.89–0.87 (t, 3H). ES-LCMS: $m/z = 536$ [M + H] $^+$.

(R)-3-Methyl-5-cyclohexylethyl-5-cyclohexylmethyl-2-iminothiohydantoin (40). $^1\text{H NMR}$ (CD_3OD): δ 3.13 (s, 3H), 1.77–1.54 (m, 14H), 1.22–1.07 (m, 9H), 1.00–0.81 (m, 5H). ES-LCMS: $m/z = 320$ [M + H] $^+$.

5,5-Diphenyl-2-iminothiohydantoin (41). A solution of benzyl (1.0 g) and *N*-methyl guanidine (0.45 g) was treated with KOH

(0.5 g) in 0.5 mL of water and 15 mL of EtOH. The resulting mixture was stirred at rt for 1 h before it was heated under reflux for 18 h. The reaction mixture was concentrated, residue diluted with water, and filtered. The solid was washed with water then recrystallized in EtOH to give 0.8 g of 5,5-diphenyl-2-iminothiohydantoin.

$^1\text{H NMR}$ (CDCl_3) δ 7.39–7.42 (m, 4H), 7.21–7.29 (m, 6H), 3.07 (s, 3H). ES-LCMS: $m/z = 266$ [M + H] $^+$.

Acknowledgment. We thank Dr. T. M. Chan and Ms. Rebecca Osterman for their help in determining multiple structures of early iminothiohydantoin, Ms. Emily Luke and Mr. Ross Yang for their help in LCMS analysis, and Drs. Catherine Strader and John Piwinski for their support of the project. Use of the IMCA-CAT beamline 17-ID and 17-BM at the Advanced Photon Source was supported by the companies of the Industrial Macromolecular Crystallography Association through a contract with the Center for Advanced Radiation Sources at the University of Chicago.

References

- (1) Part of this work was first disclosed in the following patent: Zhu, Z.; McKittrick, B.; Sun, Z.-Y.; Ye, Y.; Voigt, J.; Strickland, C.; Smith, E.; Stamford, A.; Greenlee, W.; Wu, Y.; Iserloh, U.; Mazzola, R.; Caldwell, J.; Cumming, J.; Wang, L.; Guo, T.; Le, T. X. H.; Saionz, K. W.; Babu, S. D.; Hunter, R. C. Preparation of heterocyclic aspartyl protease inhibitors for treating various diseases. Patent WO200505831, 2005.
- (2) Levy-Lehad, E.; Wijsman, E.; Nemens, E.; Anderson, A.; Goddard, K. A.; Weber, J. L. A familial Alzheimer's disease locus on chromosome 1. *Science* **1995**, *269*, 970–973.
- (3) Melnikova, I. Therapies for Alzheimer's disease. *Nat. Rev. Drug Discovery* **2007**, *6*, 341–342.
- (4) Prigerson, H. G. Costs to Society of Family Caregiving for Patients with End-Stage Alzheimer's Disease. *N. Engl. J. Med.* **2003**, *349*, 1891–1892.
- (5) Mount, C.; Downton, C. Alzheimer disease: progress or profit? *Nat. Med.* **2006**, *12*, 780–784.
- (6) Moreira, P. I.; Zhu, X.; Nunomura, A.; Smith, M. A.; Perry, G. Therapeutic Options in Alzheimer's disease. *Expert Rev. Neurother.* **2006**, *6*, 897–910.
- (7) (a) Hardy, J.; Selkoe, D. J. The Amyloid Hypothesis of Alzheimer's Disease: Progress and Problems on the Road to Therapeutics. *Science* **2002**, *297*, 353–356. (b) Haass, C.; Selkoe, D. J. Soluble protein oligomers in neurodegeneration: lessons from the Alzheimer's amyloid β -peptide. *Nat. Rev. Mol. Cell Biol.* **2007**, *8*, 101–112. (c) Korczyn, A. D. The amyloid cascade hypothesis. *Alzheimer's Dementia* **2008**, *4*, 176–178. (d) Hardy, J. Has the amyloid cascade hypothesis for Alzheimer's been proved? *Curr. Alzheimer Res.* **2006**, *3*, 71–73. (e) Selkoe, D. Alzheimer's disease: genes, proteins, and therapy. *Physiol. Rev.* **2001**, *81*, 741–766. (f) Archer, H. A.; Edison, P.; Brooks, D. J.; Barnes, J.; Frost, C.; Yeatman, T. Amyloid load and cerebral atrophy in Alzheimer's disease: a 11C-BIP positron emission tomography study. *Ann. Neurol.* **2006**, *60*, 145–147.
- (8) (a) Olson, M. I.; Shaw, C. M. Presenile dementia and Alzheimer's disease in mongolism. *Brain* **1969**, *92*, 147–156. (b) Mann, D. M. A. Alzheimer's disease and Down's syndrome. *Histopathology* **1998**, *13*, 125–137.
- (9) Prasher, V. P.; Farrer, M. J.; Kessling, A. M.; Fisher, E. M. C.; West, R. J.; Barber, S. P. C.; Butler, A. C. Molecular Mapping of IIv Alzheimer-Type Dementia in Down's Syndrome. *Ann. Neurol.* **1998**, *43*, 380–383.
- (10) (a) Pike, C. J.; Walencewicz, A. J.; Glabe, C. G.; Cotman, C. W. In vitro aging of amyloid-beta protein causes peptide aggregation and neurotoxicity. *Brain Res.* **1991**, *573*, 311–314. (b) Lorenzo, A.; Yankner, B. Beta-amyloid neurotoxicity requires fibril formation and is inhibited by congo red. *Proc. Natl. Acad. Sci. U.S.A.* **1994**, *91*, 12243–12247. (c) Iversen, L. L.; Mortishire-Sith, R. J.; Pollack, S. J.; Shearman, M. S. The toxicity in vitro of beta-amyloid protein. *Biochem. J.* **1995**, *311*, 1–16. (d) Tsai, J.; Grutzendler, J.; Duff, K.; Gan, W. Fibrillar amyloid deposition leads to local synaptic abnormalities and breakage of neuronal branches. *Nat. Neurosci.* **2004**, *7*, 1181–1183.
- (11) (a) Mor, F.; Monsonego, A. Immunization therapy in Alzheimer's disease. *Expert Rev. Neurother.* **2006**, *6*, 653–659. (b) Qu, B.; Boyer, P. J.; Johnston, S. A.; Hynan, L. S.; Rosenberg, R. N. A β 42 gene vaccination reduces brain amyloid plaque burden in transgenic mice. *J. Neurol. Sci.* **2006**, *244*, 151–158.

- (12) (a) Bayer, A. J.; Bullock, R.; Jones, R. W.; Wilkinson, D.; Paterson, K. R.; Jenkins, L. Evaluation of the safety and immunogenicity of synthetic A β 42 (AN1792) in patients with AD. *Neurology* **2005**, *64*, 94–101. (b) Gilman, S.; Koller, M.; Black, R. S.; Jenkins, L.; Griffith, S. G.; Fox, N. C. Clinical effects of A β immunization (AN1792) in patients with AD in an interrupted trial. *Neurology* **2005**, *64*, 1553–1562. (c) Hock, C.; Konietzko, U.; Streffer, J. R.; Tracy, J.; Signorell, A.; Müller-Tilmanns, B. Antibodies against b-amyloid slow cognitive decline in Alzheimer's disease. *Neuron* **2003**, *38*, 547–554. (d) Fox, N. C.; Black, R. S.; Gilman, S.; Rossor, M. N.; Griffith, S. G.; Jenkins, L. Effects of Ab immunization (AN1792) on MRI measures of cerebral volume in Alzheimer disease. *Neurology* **2005**, *64*, 1563–1572. (e) DaSilva, K. A.; Aubert, I.; McLaurin, J. Vaccine Development for Alzheimer's Disease. *Curr. Pharm. Des.* **2006**, *12*, 4283–4293.
- (13) (a) Hussain, I.; Powell, D.; Howlett, D. R.; Tew, D. G.; Meek, T. D.; Chapman, C.; Gloger, I. S.; Murphy, K. E.; Southan, C. D.; Ryan, D. M.; Smith, T. S.; Simmonds, D. L.; Walsh, F. S.; Dingwall, C.; Christie, G. Identification of a novel aspartic protease (Asp 2) as beta-secretase. *Mol. Cell Neurosci.* **1999**, *14*, 419–427. (b) D. Sinha, S.; Anderson, J. P.; Barbour, R.; Basl, G. S.; Caccavello, R.; Davis, D.; Doan, M.; Dovey, H. F.; Frigon, N.; Hong, J.; Jacobson-Croak, K.; Jewett, N.; Keim, P.; Knops, J.; Lieberburg, I.; Power, M.; Tan, H.; Tatsuno, G.; Tung, J.; Schenk, D. Purification and cloning of amyloid precursor protein betasecretase from human brain. *Nature* **1999**, *402*, 537–540. (c) Vassar, R.; Bennett, B. D.; Babu-Khan, S.; Kahn, S.; Mendiaz, E. A.; Denis, P.; Teplow, D. B.; Ross, S.; Amarante, P.; Loeloff, R.; Luo, Y.; Fisher, S.; Fuller, J.; Edenson, S.; Lile, J.; Jarosinski, M. A.; Biere, A. L.; Curran, E.; Burgess, T.; Louis, J. C. Beta-secretase cleavage of Alzheimer's amyloid precursor protein by the transmembrane aspartic protease BACE. *Science* **1999**, *286*, 735–741. (d) Yan, R.; Bienkowski, M. J.; Shuck, M. E.; Miao, H.; Tory, M. C.; Pauley, A. M.; Brashers, J. R.; Stratman, N. C.; Mathews, W. R.; Buhl, A. E.; Carter, D. B.; Tomasselli, A. G.; Parodi, L. A.; Heinrikson, R. L.; Gurney, M. E. Membrane-anchored aspartyl protease with Alzheimer's disease beta-secretase activity. *Nature* **1999**, *402*, 533–537.
- (14) (a) Luo, Y.; Bolon, B.; Kahn, S.; Bennett, B. D.; Babu-Khan, S.; Denis, P.; Fan, W.; Kha, H.; Zhang, J.; Gong, Y.; Martin, L.; Louis, J. C.; Yan, Q.; Richards, W. G.; Citron, M.; Vassar, R. Mice deficient in BACE1, the Alzheimer's betasecretase, have normal phenotype and abolished beta-amyloid generation. *Nat. Neurosci.* **2001**, *4*, 231–232. (b) Luo, Y.; Bolon, B.; Damore, M. A.; Fitzpatrick, D.; Liu, H.; Zhang, J.; Yan, Q.; Vassar, R.; Citron, M. BACE1 (beta-secretase) knockout mice do not acquire compensatory gene expression changes or develop neural lesions over time. *Neurobiol. Dis.* **2003**, *14*, 81–88.
- (15) (a) Willem, M.; Garratt, A. N.; Novak, B.; Citron, M.; Kaufmann, S.; Rittger, A.; DeStrooper, B.; Saftig, P.; Birchmeier, C.; Haass, C. Control of Peripheral Nerve Myelination by the b-Secretase BACE1. *Science* **2006**, *314*, 664–666. (b) Wang, H.; Song, L.; Laird, F.; Wong, P. C.; Lee, H.-K. BACE1 Knock-Outs Display Deficits in Activity-Dependent Potentiation of Synaptic Transmission at Mossy Fiber to CA3 Synapses in the Hippocampus. *J. Neurosci.* **2008**, *28*, 8677–8681.
- (16) Ohno, M.; Sametsky, E. A.; Younkin, L. H.; Oakley, H.; Younkin, S. G.; Citron, M.; Vassar, R.; Disterhoft, J. F. BACE1 deficiency rescues memory deficits and cholinergic dysfunction in a mouse model of Alzheimer's disease. *Neuron* **2004**, *41*, 27–33.
- (17) (a) Farzan, M.; Schnitzler, C. E.; Vasilieva, N.; Leung, D.; Choe, H. BACE2, a beta-secretase homolog, cleaves at the beta site and within the amyloid-beta region of the amyloid-beta precursor protein. *Proc. Natl. Acad. Sci. U.S.A.* **2000**, *97*, 9712–9717. (b) Saunders, A. J.; Kim, T.-M.; Tanzi, R. E. BACE Maps to Chromosome 11 and a BACE Homolog, BACE2, Reside in the Obligate Down Syndrome Region of Chromosome 21. *Science* **1999**, *286*, 1255a.
- (18) (a) Sidera, C.; Liu, C.; Austen, B. Pro-domain removal in ASP-2 and the cleavage precursor are influenced by pH. *BMC Biochem.* **2002**, *3*, 25–37, www.biomedcentral.com. (b) The optimum pH profile was later confirmed: Stachel, S. J.; Coburn, C. A.; Rush, D.; Jones, K. L. G.; Zhu, H.; Rajapakse, H.; Graham, S. L.; Simon, A.; Holloway, M. K.; Allison, T. J.; Munshi, S. K.; Espeseth, A. S.; Zuck, P.; Colussi, D.; Wolfe, A.; Pietrak, B. L.; Lai, M.-T.; Vacca, J. P. Discovery of aminoheterocycles as a novel b-secretase inhibitor class: pH dependence on binding activity part 1. *Bioorg. Med. Chem. Lett.* **2009**, *19*, 2977–2980. However, in our hands, the BACE1 cellular IC₅₀ and enzyme Ki can be in good agreement at the in vitro assay pH (5) depending on the inhibitor structures and other factors such as pep efflux activities.
- (19) (a) Stachel, S. J. Progress toward the development of a viable BACE-1 inhibitor. *Drug Dev. Res.* **2009**, *70*, 101–110. (b) Durham, T. B.; Shepherd, T. A. Progress toward the discovery and development of efficacious BACE inhibitors. *Curr. Opin. Drug Discovery Dev.* **2006**, *9*, 776–791.
- (20) Ghosh, A. K.; Shin, D.; Downs, D.; Koelsch, G.; Lin, X.; Ermoloeff, J.; Tang, J. Design of Potent Inhibitors for Human Brain memapsin 2 (β -Secretase). *J. Am. Chem. Soc.* **2000**, *122*, 3522–3523.
- (21) (a) Maillard, M.; Hom, C.; Gailunas, A.; Jagodzinska, B.; Fang, L. Y.; Vargese, J.; Freskos, J. N.; Pulley, S. R.; Beck, J. P.; Tenbrink, R. E. Compounds to treat Alzheimer's disease. Patent WO2002002512, **2002**; (b) Maillard, M. C.; Hom, R. K.; Benson, T. E.; Moon, J. B.; Mamo, S.; Bienkowski, M.; Tomasselli, A. G.; Woods, D. D.; Prince, D. B.; Paddock, D. J.; Emmons, T. L.; Tucker, J. A.; Dappen, M. S.; Brogley, L.; Thorsett, E. D.; Jewett, N.; Sinha, S.; Varghese, J. Design, Synthesis, and Crystal Structure of Hydroxyethyl Secondary Amine-Based Peptidomimetic Inhibitors of Human β -Secretase. *J. Med. Chem.* **2007**, *50*, 776–781.
- (22) (a) Hyland, L. J.; Tmaszek, T. A., Jr.; Meek, T. D. Human immunodeficiency virus-1 protease. 2. Use of pH rate studies and solvent kinetic isotope effects to elucidate details of chemical mechanism. *Biochemistry* **1991**, *30*, 8454–8463. (b) For a general review on this topic: Bursavich, M. G.; Rich, D. H. *J. Med. Chem.* **2002**, *45*, 541–558. (c) Toulkhonova, L.; Metzler, W. J.; Witmer, M. R.; Copeland, R. A.; Marcinkeviciene, J. Kinetic Studies on beta-Site Amyloid Precursor Protein-Cleaving Enzyme (BACE). *J. Biol. Chem.* **2003**, *278*, 4582–4589.
- (23) Silvestri, R. Boom in the development of non-peptidic beta-secretase (BACE1) inhibitors for the treatment of Alzheimer's disease. *Med. Res. Rev.* **2009**, *29*, 295–338 and references therein.
- (24) Wang, Y.-S.; Strickland, C.; Voigt, J. H.; Kennedy, M. E.; Beyer, B. M.; Senior, M. M.; Smith, E. M.; Nechuta, T. L.; Madison, V. S.; Czarniecki, M.; McKittrick, B. A.; Stamford, A. W.; Parker, E. M.; Hunter, J. C.; Greenlee, W. J.; Wyss, D. F.; Application of Fragment-Based NMR Screening, X-ray Crystallography, Structure-Based Design, and Focused Chemical Library Design to Identify Novel μ M Leads for the Development of nM BACE-1 (β -site APP Cleaving Enzyme 1) Inhibitors. *J. Med. Chem.* **2010**, *53*, DOI: 10.1021/jm901472u.
- (25) Albert, A.; Goldacre, R.; Phillips, J. The Strength of Heterocyclic Bases. *J. Chem. Soc.* **1948**, 2240–2249.
- (26) See ref 23b for more detailed discuss about the flap and its conformations.
- (27) (a) Detailed description of the protonation states will be a subject of another publication. (b) It was suggested that the most stable protonation state for the apo-protein is the deprotonated state Rajamani, R.; Reynolds, C. H. Modeling the Protonation States of the Catalytic Aspartates in beta-Secretase. *J. Med. Chem.* **2004**, *47*, 5159–5166.
- (28) (a) Hueper, W. C.; Ichniowsky, C. T. Toxicopathologic studies on S-methylisothiourea. *Virchows Arch. Pathol. Anat. und Physiol. Klin. Med.* **1944**, *37*, 253–263. (b) Dieke, S. H.; Allen, G. S.; Richter, C. P. The acute toxicity of thioureas and related compounds to wild and domestic Norway rats. *J. Pharmacol.* **1947**, *90*, 260–270.
- (29) Peterlin-Masic, L.; Cesar, J.; Zega, A. Metabolism-Directed Optimisation of Antithrombotics: The Prodrug Principle. *Curr. Pharm. Des.* **2006**, *12*, 73–91.
- (30) (a) Lipinski, C. A.; Lombardo, F.; Dominy, B. W.; Feeney, P. J. Experimental and computational approaches to estimate solubility and permeability in drug discovery and development settings. *Adv. Drug Delivery Rev.* **2001**, *46*, 3–26. (b) Veber, D. F. et al. Molecular properties that influence the oral bioavailability of drug candidates. *J. Med. Chem.* **2002**, *45*, 2615–2623. (c) Lipinski, C. A. Lead- and drug-like compounds: the rule-of-five revolution. *Drug Discovery Today: Technol.* **2004**, *1*, 337–341.
- (31) See ref 26.
- (32) (a) Grazybowski, A. K.; Datta, S. P. The ionization constant of the protonated form of creatinine. *J. Chem. Soc.* **1964**, 187–196. (b) Winiwarter, S.; Bonham, N. M.; Ax, F.; Hallberg, A.; Lenneras, H.; Karlen, A. Correlation of human jejunal permeability (in vivo) of drugs with experimentally and theoretically derived parameters. A multivariate data analysis approach. *J. Med. Chem.* **1998**, *41*, 4939–4949.
- (33) Lindel, T.; Hoffmann, H. Synthesis of dispacamide from the marine sponge *Agelas dispar*. *Tetrahedron Lett.* **1997**, *38*, 8935–8938.
- (34) For an example: Ishizumi, K.; Ohashi, N.; Tanno, N. Stereospecific total synthesis of 9-aminoanthracyclines: (+)-9-amino-9-deoxydaunomycin and related compounds. *J. Org. Chem.* **1987**, *52*, 4477–4485.
- (35) Altmann, E.; Nebel, K.; Mutter, M. Versatile stereoselective synthesis of completely protected trifunctional alpha-methylated alpha-amino acid starting from alanine. *Helv. Chim. Acta* **1991**, *74*, 800–806.

- (36) Short, K. M.; Ching, B. W.; Majali, A. M. M. Exploitation of the Ugi 4CC reaction: preparation of small molecule combinatorial libraries via solid phase. *Tetrahedron* **1997**, *53*, 6653–6679.
- (37) For experimental procedure of pK_a measurements: Caliaro, G. A.; Herbots, C. A. Determination of pK_a values of basic new drug substances by CE. *J. Pharm. Biomed. Anal.* **2001**, *26*, 427–434.
- (38) (a) SAR study regarding to the interaction associated with this site will be a subject of another publication. (b) This site was later disclosed by the following publication: Steele, T. G.; Hills, I. D.; Nomland, A. A.; Leon de, P.; Allison, T.; McGaughey, G.; Colussi, D.; Tugusheva, K.; Haugabook, S. J.; Espeseth, A. S.; Zuck, P.; Graham, S. L.; Stachel, S. J. Identification of a small molecule b-secretase inhibitor that binds without catalytic aspartate engagement. *Bioorg. Med. Chem. Lett.* **2009**, *19*, 17–20.
- (39) (a) Tonelli, A. E. On the stability of cis and trans amide bond conformations in polypeptides *J. Am. Chem. Soc.* **1971**, *93*, 7153–7155 and references therein. (b) Based on an ab initio calculation, the S-cis conformation is 1 kcal/mol higher in energy than the S-trans one.
- (40) Hopkins, A. L.; Groom, C. R.; Alex, A. Ligand efficiency: a useful metric for lead selection. *Drug Discovery Today* **2004**, *9*, 430–431.
- (41) Korfmacher, W. A.; Cox, K. A.; Ng, K. J.; Veals, J.; Hsien, Y.; Wainhaus, S.; Broske, L.; Prelusky, D.; Nomeir, A.; White, R. E. Cassette-accelerated rapid rat screen: a systematic procedure for the doing and liquid chromatography/atmospheric pressure ionization tandem mass spectrometric analysis of new chemical entities as part of new drug discovery. *Rapid Commun. Mass. Spectrom.* **2001**, *15*, 335–340.
- (42) In fact, a similar strategy was employed by the discovery team that identified the peptidomimetic renin inhibitor, Aliskiren. (A) Göschke, R.; Cohen, N. C.; Wood, J. M.; Maibaum, J. Design and synthesis of novel 2,7-dialkyl substituted 5(S)-amino-4(S)-hydroxy-8-phenyl-octanecarboxamides as in vitro potent peptidomimetic inhibitors of human rennin. *Bioorg. Med. Chem. Lett.* **1997**, *7*, 2735–2740. (b) Maibaum, J.; Stutz, S.; Göschke, R.; Rigollier, P.; Yamaguchi, Y.; Cumin, F.; Rahuel, J.; Baum, H.-P.; Cohen, N.-C.; Schnell, C. R.; Fuhrer, W.; Gruetter, M. G.; Schilling, W.; Wood, J. M. Structural Modification of the P2' Position of 2,7-Dialkyl-Substituted 5(S)-Amino-4(S)-hydroxy-8-phenyl-octanecarboxamides: The Discovery of Aliskiren, a Potent Nonpeptide Human Renin Inhibitor Active after Once Daily Dosing in Marmosets. *J. Med. Chem.* **2007**, *50*, 4832–4844.
- (43) Yasuda, Y.; Kageyama, T.; Akamine, A.; Shibata, M.; Kominami, E.; Uchiyama, Y.; Yamamoto, K. Characterization of new fluorogenic substrates for the rapid and sensitive assay of cathepsin E and cathepsin D. *J. Biochem.* **1999**, *125*, 1137–1143.
- (44) see ref 1 for the patent covering compounds discussed in this manuscript.
- (45) (a) Cole, D. C.; Manas, E. S.; Stock, J. R.; Condon, J. S.; Jennings, L. D.; Aulabaugh, A.; Chopra, R.; Cowling, R.; Ellingboe, J. W.; Fan, K. Y.; Harrison, B. L.; Hu, Y.; Jacobsen, S.; Jin, G.; Lin, L.; Lovering, F. E.; Malamas, M.; Stahl, M. L.; Strand, J.; Sukhdeo, M. N.; Svenson, K.; Turner, M. J.; Wagner, E.; Wu, J.; Zhou, P.; Bard, J. Acylguanidines as Small-Molecule beta-Secretase Inhibitors. *J. Med. Chem.* **2006**, *49*, 6158–6161. (b) Malamas, M. S.; Erdei, J. J.; Gunawan, I. S.; Zhou, P.; Yan, Y. Quagliato, D. A. Amino-5,5-diphenylimidazolone derivatives for the inhibition of beta-secretase. U.S. Patent US20050282825, **2005**.
- (46) (a) Murray, C. W.; Callaghan, O.; Chessari, G.; Cleasby, A.; Congreve, M.; Frederickson, M.; Hartshorn, M. J.; McMenamin, R.; Patel, S.; Wallis, N. Application of Fragment Screening by X-ray Crystallography to beta-Secretase. *J. Med. Chem.* **2007**, *50*, 1116–1123. (b) Congreve, M.; Aharony, D.; Albert, J.; Callaghan, O.; Campbell, J.; Carr, R. A. E.; Chessari, G.; Cowan, S.; Edwards, P. D.; Frederickson, M.; McMenamin, R.; Murray, C. W.; Patel, S.; Wallis, N. Application of Fragment Screening by X-ray Crystallography to the Discovery of Aminopyridines as Inhibitors of beta-Secretase. *J. Med. Chem.* **2007**, *50*, 1124–1132. (c) Geschwindner, S.; Olsson, L.-L.; Albert, J. S.; Deinum, J.; Edwards, P. D.; de Beer, T.; Folmer, R. H. A. Discovery of a Novel Warhead against beta-Secretase through Fragment-Based Lead Generation. *J. Med. Chem.* **2007**, *50*, 5903–5911. (d) Edwards, P. D.; Albert, J. S.; Sylvester, M.; Aharony, D.; Andisik, D.; Callaghan, O.; Campbell, J. B.; Carr, R. A.; Chessari, G.; Congreve, M.; Frederickson, M.; Folmer, R. H. A.; Geschwindner, S.; Koether, G.; Kolmodin, K.; Krumrine, J.; Mauger, R. C.; Murray, C. W.; Olsson, L.-L.; Patel, S.; Spear, N.; Tian, G. Application of fragment-based lead generation to the discovery of novel, cyclic amidine beta-secretase inhibitors with nanomolar potency, cellular activity, and high ligand efficiency. *J. Med. Chem.* **2007**, *50*, 5912–5925. (e) Albert, J. S.; Andisik, D.; Arnold, J.; Brown, D.; Callaghan, O.; Campbell, J.; Carr, R. A. E.; Chessari, G.; Congreve, M. S.; Edwards, P.; Empfield, J. R.; Frederickson, M.; Koether, G. M.; Krumrine, J.; Mauger, R.; Murray, C. W.; Patel, S.; Sylvester, M.; Throner, S. Substituted Amino-Compound and Uses thereof. Patent WO2006041404, **2006**.
- (47) For an example, an X-ray cocrystal structure of t-RNA-guanine transglycosylase inhibitor that features a 2-aminopyrimidinone interacting with two aspartic acid (ASP^{102} and ASP^{136}), in a fashion similar to **3** and BACE1, was reported: Brenk, R.; Meyer, E. A.; Reuter, K.; Stubbs, M. T.; Garcia, G. A.; Diederich, F.; Klebel, G. Crystallographic Study of Inhibitors of tRNA-guanine Transglycosylase Suggests a New Structure-Based Pharmacophore for Virtual Screening. *J. Mol. Biol.* **2004**, *338*, 55–75.
- (48) Congreve, M.; Carr, R.; Murray, C.; Jhoti, H. A “Rule of three” for fragment-based lead discovery? *Drug Discovery Today* **2003**, *8*, 876–877.
- (49) *Jaguar*, version 5.5; Schrödinger LLC: New York.
- (50) Kennedy, M. E.; Wang, W.; Song, L.; Lee, J.; Zhang, L.; Wong, G.; Wang, L.; Parker, E. Measuring Human Beta-Secretase (BACE1) Activity Using Homogeneous Time-Resolved Fluorescence. *Anal. Biochem.* **2003**, *319*, 49–55.